Available online at www.sciencedirect.com
ScienceDirect
Engineering Geology 88 (2006) 173 – 199
ENGINEERING GEOLOGY
www.elsevier.com/locate/enggeo

Investigating landslides with space-borne Synthetic Aperture Radar (SAR) interferometry

Carlo Colesanti [1], Janusz Wasowski [a,*]

[a] *CNR-IRPI, Bari, Italy*

Accepted 11 September 2006
Available online 15 November 2006

Abstract

This paper is addressed to readers without advanced knowledge of remote sensing. It illustrates some current and potential uses of satellite Synthetic Aperture Radar interferometry (InSAR) for landslide assessment. Data acquired by SAR systems can provide 3D terrain models and be used to assist in regional scale investigations, e.g. aimed at evaluation of susceptibility of slopes to failure. Under favourable environmental conditions, the innovative Permanent Scatterers (PS) technique, which overcomes several limitations of conventional SAR differential interferometry (DInSAR) applications in landslide studies, is suitable for monitoring slope deformations with millimetric precision. The PS technique combines the wide-area coverage typical of satellite imagery with the capability of providing displacement data relative to individual image pixels. With the currently available radar satellites, however, only very slow ground surface displacements can be reliably detected and measured. The presented case study of a landslide from the Liechtenstein Alps indicates that the most attractive and reliable contribution provided by this remote sensing technique lies in the possibility of (i.) wide-area qualitative distinction between stable and unstable areas and (ii.) qualitative (relative) hazard zonation of large, slow landslides based on the identification of segments characterised by different movement rates. Since only the radar line of sight projection of the displacements can be detected, a quantitative exploitation of the PS data is possible only where sufficient ground truth is available. In site specific or single landslide investigations the PS data can represent a very useful complementary data source with respect to the information acquired through ground based observations and in situ surveying. However, the difficulties associated with the feasibility assessments of the applicability of SAR data to local scale problems, as well as with the interpretation of PS results, require a close collaboration between landslide experts and specialists in advanced processing of radar satellite data. The interpretation of the exact geotechnical significance of small, radar sensed ground surface deformations is challenging, especially where ground truth is lacking. Although any ground deformation is potentially of interest to an engineering geologist, detection of movements in both vertical and horizontal directions is needed in the case of landslides to evaluate slope failure mechanisms. With their high radar viewing angles, however, the current space-borne systems can detect only a fraction of the horizontal component of movement. It is expected that the upcoming SAR dedicated missions with new sensors and different acquisition geometries, combined with the rapid developments in the field of advanced radar data processing, will allow a full 3D reconstruction of deformation data and help to further reduce the current limitations of the PS and similar DInSAR approaches.

Keywords: Landslide; Satellite Remote Sensing; Synthetic Aperture Radar; Interferometry; Permanent Scatterers; Liechtenstein

* Corresponding author. Fax: +39 080 5929610.
E-mail address: j.wasowski@ba.irpi.cnr.it (J. Wasowski).
[1] Formerly with Dipartimento di Elettronica e Informazione, Politecnico di Milano and with Tele-Rilevamento Europa-T.R.E. Srl, Milano, Italy.

0013-7952/$ - see front matter © 2006 Elsevier B.V. All rights reserved.
doi:10.1016/j.enggeo.2006.09.013

1. Introduction

Recent years have witnessed an increasing number of initiatives and studies aimed at demonstrating the applicability of Earth Observation (EO) satellite data for slope instability investigations (e.g. CEOS DMSG, 2002; Wasowski and Singhroy, 2003; IGOS GEOHAZARDS, 2004, and references therein). This appears to have resulted from i) the greater data availability thanks to several launches of both radar and optical space-borne platforms (e.g. European ERS-1 and ERS-2 satellites, Japanese JERS-1, Canadian RADARSAT, United States LANDSAT TM, European ENVISAT, as well as commercial satellites such as IKONOS, QUICKBIRD), ii) the improved capabilities of the space sensors and iii) the development of more advanced EO data processing techniques.

The focus of this work is on radar sensors because their potential and practical applications are generally less well known in the engineering geology community with respect to those related to the use of optical systems. Indeed, the progress in differential Synthetic Aperture Radar interferometry (DInSAR), a technique capable of generating wide-area maps of ground surface deformations measured with millimeter precision (e.g. Gabriel et al., 1989; Ferretti et al., 2000a), has recently attracted much attention of researchers and practitioners involved in landslide monitoring and hazard assessment. This has been stimulated by some successful case studies, which indicated the potential of DInSAR in the detection of landslide movements (e.g. Fruneau et al., 1996; Rott et al., 1999; Kimura and Yamaguchi, 2000; Nagler et al., 2002; Berardino et al., 2003; Colesanti et al., 2003a; Colesanti and Wasowski, 2004; Farina et al., 2004; Hilley et al., 2004; Singhroy and Molch, 2004; Strozzi et al., 2005; Bovenga et al., 2006-this issue), as well as through a series of workshops and demonstration projects supported by space agencies e.g. European Space Agency's (ESA) projects MASMOV, ALPS, SLAM (see http://dup.esrin.esa.it).

However, significant challenges persist regarding the practical applicability of satellite radar data to landslide investigations (e.g. Carnec et al., 1996; Singhroy et al., 1998; Wasowski and Gostelow, 1999; CEOS DMSG, 2002; Wasowski et al., 2002). Coherence loss, a problem typical of vegetated areas, and atmospheric effects are the most important factors that limit the utility of many currently available radar satellite datasets. These difficulties can be in part overcome by using innovative DInSAR techniques (e.g. Ferretti et al., 2001a; Lanari et al., 2004) and exploiting long series of SAR images. Also, the upcoming launches of new satellite systems, with higher resolution sensors (e.g. RADARSAT 2) or working in the lower frequency L-band (e.g. ALOS), which seems more suitable for landslide applications (e.g. Strozzi et al., 2005), appear promising and hold the premise for increasing practical use of radar satellite data in landslide investigations. In the meantime, however, there is a risk that the insufficient appreciation of inherent limitations of EO systems and relevant processing techniques, coupled with natural complexities of landslide movements and related ground deformation phenomena, may result in misinterpretations of satellite SAR data.

To foster the awareness of the utility and limitations of radar-based remote sensing, we present a review of the basic principles of SAR interferometry and relevant processing techniques and offer also comprehensive information on a new Permanent Scatterers (PS) DInSAR technique (Ferretti et al., 2000a, 2001a; Colesanti et al., 2003b). We stress practical aspects of radar interferometry (e.g. output products, advantages, limitations), as the information is addressed to a reader without advanced knowledge in remote sensing processing. Then, the paper describes some of the current and potential applications of radar satellite imagery for slope instability assessments. We provide examples of how radar data can be exploited to produce interferometric digital elevation models (DEMs), useful for wide-area preliminary assessments of susceptibility of slopes to failure, and to detect and quantify slow landslide movements through the application of the PS DInSAR. To illustrate the capabilities and limitations of space-borne SAR, with particular reference to the exploitation of the two SAR sensors mounted on the ERS-1and ERS-2 satellites, we present the case study of a large Triesenberg–Triesen landslide located in the Liechtenstein Alps (Fig. 1). Some significant remotely sensed ground surface deformations are discussed in the context of the local site conditions and slope processes to indicate how the radar interferometry monitoring can complement conventional in situ landslide investigations.

2. Principles of space-borne Synthetic Aperture Radar (SAR)

Here we offer only a brief introduction to space-borne SAR. Further details, including principles of SAR data acquisition, processing and analysis, as well as reviews of applications can be found in radar remote sensing literature (e.g. Henderson and Lewis, 1998; Franceschetti and Lanari, 1999; Hanssen, 2001).

Synthetic Aperture Radar (SAR) is an active microwave device capable of recording the electromagnetic

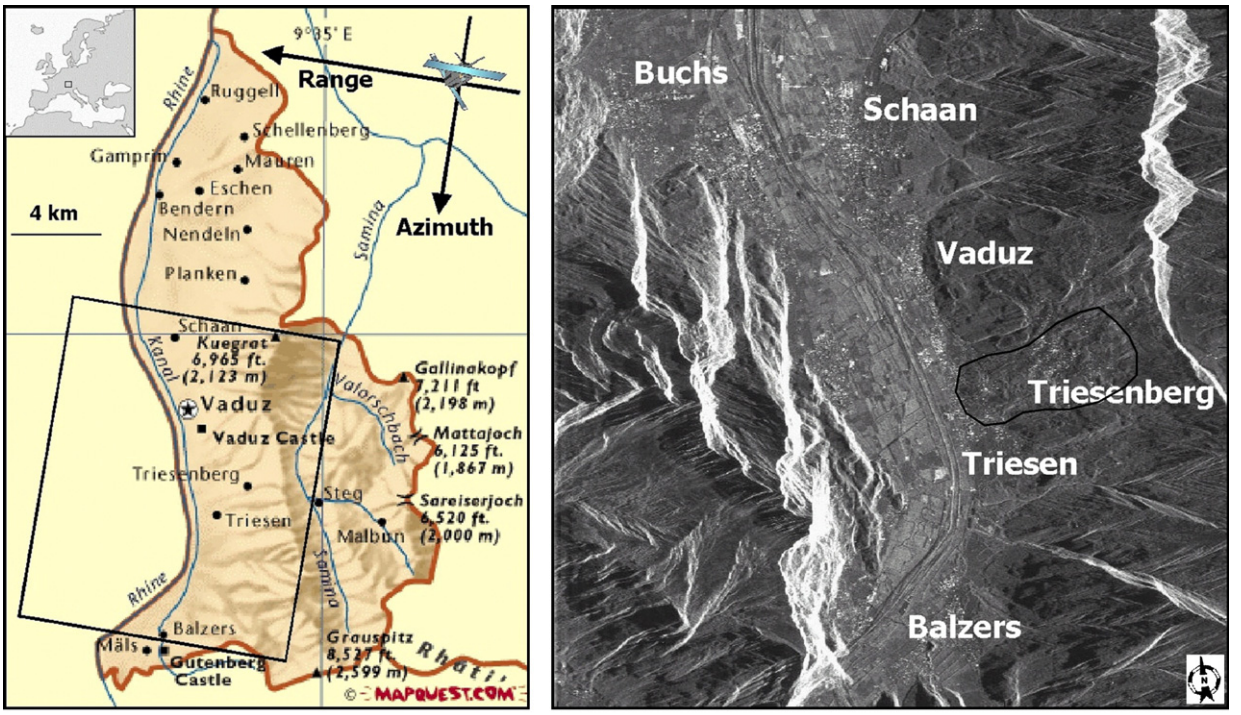

Fig. 1. Cartographic base map of Liechtenstein (left) and SAR multi-image reflectivity image (right) of the Rhine River valley area including the Triesenberg–Triesen landslide site (marked by black line). Note also a satellite sketch with black arrows indicating radar azimuth and range directions.

echo backscattered from the Earth surface and of arranging it in a 2D image map, whose dimensions are the sensor-target distance (slant range or Line of Sight direction, LOS) and the platform flight direction (azimuth). With respect to optical sensors SAR offers several unique opportunities, but also presents considerable data processing and interpretation difficulties.

Being an active system, SAR is independent of Sun illumination. Moreover, microwaves can penetrate clouds, and, to some extent (up to several cm, depending on the operating frequency) even soil, vegetated canopies, and snow.

One of the currently operating space-borne radar systems is the ESA ERS-2 satellite, whose side-looking SAR sensor images the Earth from an orbit about 780 km above the Earth surface. ERS-2 images a 100 km wide strip (swath) with a constant off-nadir angle (strip map mode) of around 21° (at mid-range). The ERS orbit is nearly polar and data are acquired both along ascending and descending orbits, respectively moving from approximately south towards north and vice versa. In the case of a flat terrain, the incidence angle θ, varying from 19° (near range) to 26° (far range), is slightly larger than the off-nadir angle due to the curvature of the Earth surface.

The ERS acquisition geometry and the main parameters (in particular the incidence angle θ and the off-nadir angle) are sketched in Fig. 2A and B. In its principal acquisition mode, ERS-2 offers global coverage with a 35 day revisiting time, i.e. it overpasses the same area with the same nominal acquisition geometry every 35 days. ERS-2 operates in vertical (VV) polarisation in C band (carrier frequency 5.3 GHz); the data are compatible (for SAR image processing) with those acquired by ERS-1 during its operating life from July 1991 to March 2000. (It is worth remarking that also ENVISAT in its image mode has very similar acquisition parameters).

SAR systems are coherent, i.e. capable of recording both amplitude and phase values. Therefore, a focused SAR image is a complex valued matrix. Its amplitude is a map of the (microwave) ground reflectivity of the sensed area (ERS scenes cover approximately a 100×100 km^2 area). On the other hand, the SAR phase depends both on the local reflectivity and on the sensor-target distance. The sensitivity of phase data to the sensor-target distance is extremely high: a two way path difference of λ, i.e. a single way path difference of 0.5λ (=2.83 cm for ERS and RADARSAT) translates into a full phase cycle (2π).

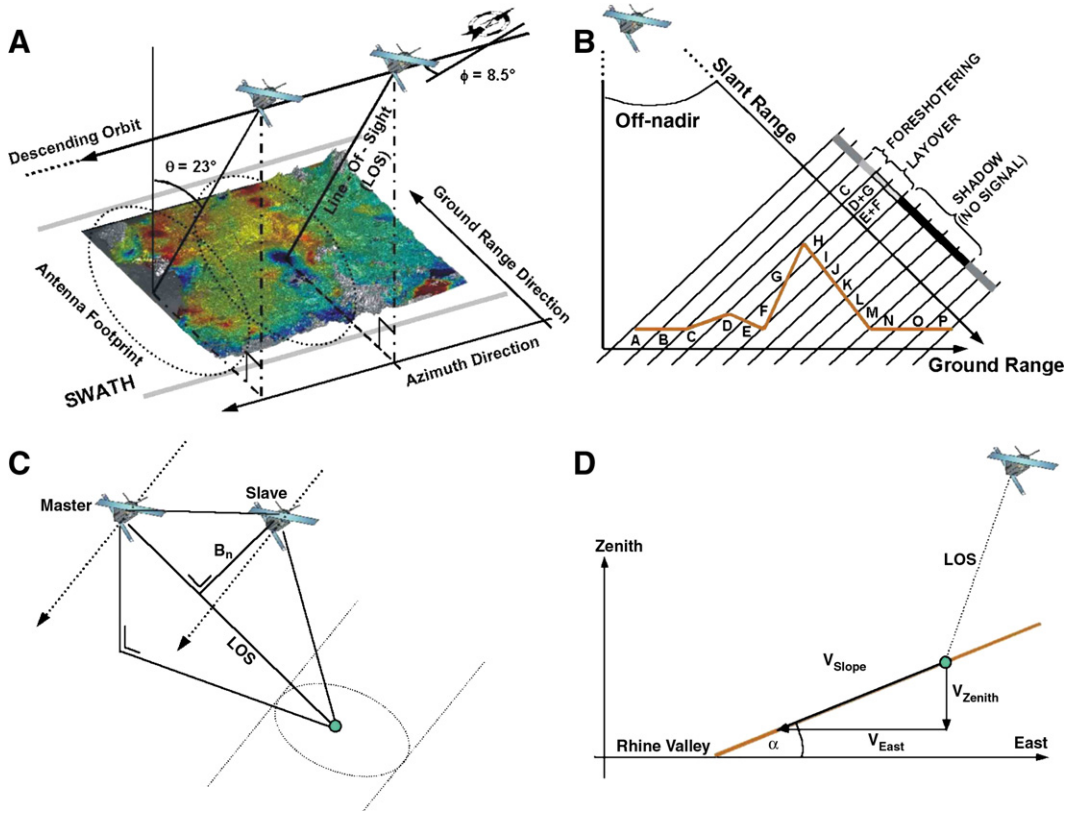

Fig. 2. A) ERS acquisition geometry; B) Geometric distortion effects: foreshortening (range pixel C), layover (range pixels D, G, E, F) and shadowing (range pixels H–N), (plot based on Monti Guarnieri, 2002); C) Simplified geometry of interferometric measurements; D) Slope aspect and inclination at the Triesenberg–Triesen landslide site, Liechtenstein (LOS: Line-Of-Sight; B_n: normal baseline).

The resolution of ERS imagery amounts to about $\Delta az = 5$ m in azimuth direction and $\Delta sr = 9.5$ m in slant range. Depending on the local topography this last figure corresponds to a ground range resolution Δgr of:

$$\Delta gr = \frac{\Delta sr}{\sin(\theta - \alpha)}$$

where θ is the local incidence angle and α the local terrain slope (α is positive for slopes dipping towards the sensor and negative for slopes dipping away from the sensor). For flat terrain ($\alpha = 0°$) at mid-range ($\theta = 23°$), the ground range resolution is about 25 m.

The resolution should not be confused with the sampling step (i.e. the actual size of a single image pixel) that is slightly finer: in azimuth 4 m, in slant range 8 m and, therefore, 20 m in ground range (flat terrain, mid-range). We recall that an imaging system solves correctly two objects as long as it is capable to recognise that their contributions are relative to two different elements and not to a unique target.

The radar "ranging" mechanism induces a slope dependent resolution (and pixel size) along ground range. This is responsible for well known geometric distortion effects (Fig. 2B), which need to be taken into account before attempting the exploitation of SAR data in engineering geological investigations, especially in those concerning slope instability:

- Foreshortening, whereby slopes facing the sensor ($0 < \alpha < \theta$) are compressed in a few image pixels with bright reflectivity, representing a sum of signal contributions relative to scattering elements spread in a larger sampling cell. Such slopes are imaged with a considerably worse resolution (and sampling step) than flat terrain. A worst condition occurs when a slope has constant inclination and $\alpha = \theta$. Such a slope would be imaged in a unique range pixel regardless of its actual areal extension. Moreover, if the inclination exceeds θ, top and bottom of the slope are inverted on the SAR image. This is the so-called layover effect.

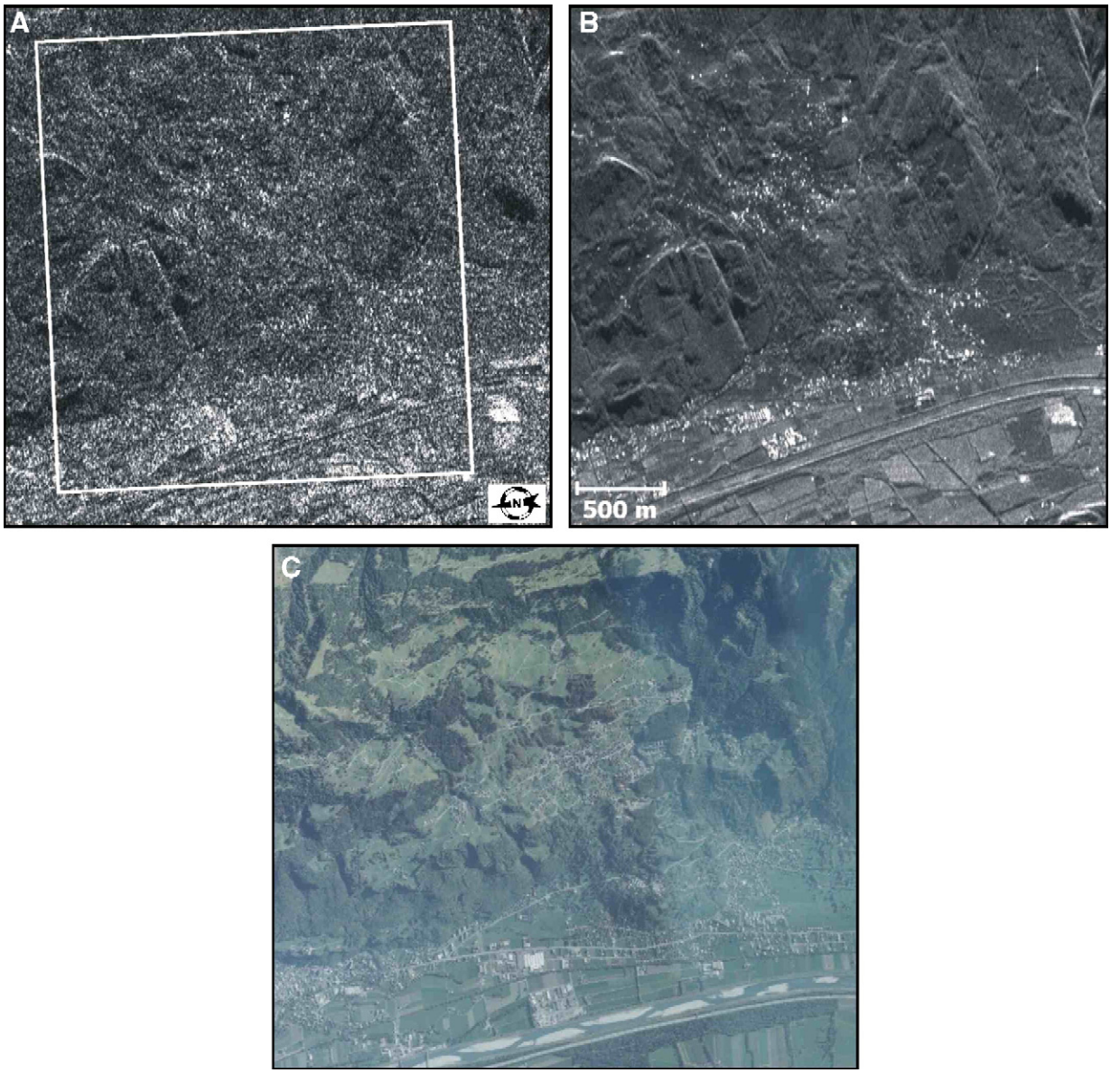

Fig. 3. Comparison of SAR imagery and an aerial photograph showing the area affected by the Triesenberg–Triesen landslide (situated in the centre of three images). A) Single-image reflectivity map (no speckle removal spatial filtering) in SAR co-ordinates. The white rectangle marks approximately the area shown in Fig. C; B) Multi-image reflectivity map (speckle removal by means of pixel by pixel incoherent averaging, without loss of resolution) in SAR co-ordinates; C) Aerial orthorectified photo (property of Tiefbauamt Vaduz).

- On the other hand, slopes facing away from the SAR sensor ($-(90\text{-}\theta)<\alpha<0$) are imaged at a higher resolution than flat terrain. However, steep slopes whose inclination exceeds ($90-\theta$), and the area immediately behind them, are not illuminated at all by the radar signal. This is known as the shadow effect.

Obviously, SAR amplitude and phase data are of very limited use in areas affected by foreshortening and cannot be profitably exploited in areas affected by shadowing and layover.

Another phenomenon influencing the quality of SAR imagery is speckle, a direct consequence of the coherent imaging capability of SAR sensors (Fig. 3A). The complex value attributed to each image pixel is actually the coherent sum of the contributions relative to all scattering elements within the same sampling cell. This leads to a random (Rayleigh distributed) amplitude

value for each SAR sampling cell in which the various terms can be considered mutually independent and no individual scatterer dominates the other elements (e.g. vegetated areas, water surfaces).

Since the speckle effect is induced by the image formation mechanism (i.e. coherent sum of contributions), the only way to reduce speckle is by averaging. However, averaging carried out in space within a single image leads unavoidably to a loss of resolution.

If enough SAR images are available and if they are re-sampled on a common grid and radiometrically corrected, a pixel by pixel inter-image incoherent averaging (i.e. averaging amplitude values) reduces speckle without any loss of resolution (Ferretti et al., 2001a), as depicted in Fig. 3B. Clearly this technique of generating multi-image reflectivity maps is meaningful as long as no significant reflectivity variation is expected within the observation time span.

If speckle can be suitably reduced, amplitude SAR imagery represents a potentially very useful source of information, which can complement high resolution optical imagery and aerial photography, e.g. in feature detection. A relevant advantage is that SAR imagery is not affected by effects (mainly shadows) induced by the particular position of the Sun during the acquisition. However, the relatively low spatial resolution of currently available space-borne SAR data represents a significant practical limitation.

3. SAR interferometry

3.1. Background

Here we briefly review the basic principles of SAR interferometry (InSAR) and address its potential and main limitations. The interested reader can find additional information in books (e.g. Henderson and Lewis, 1998; Franceschetti and Lanari, 1999; Hanssen, 2001), as well as in review papers (e.g. Massonnet and Feigl, 1998; Rosen et al., 2000).

The basic principle of interferometry relies on the fact that the phase of SAR images is an ambiguous (modulo-2π) measure of the sensor-target distance. Distance variations can, therefore, be determined by computing on a pixel by pixel basis the phase difference (interferometric phase) relative to two SAR images. This is actually performed as pixel by pixel product of the reference image (master) times the complex conjugated secondary (slave) image.

As already mentioned, each SAR image pixel represents the coherent sum of all scattering elements within a resolution cell. Moreover, each element contributes both with its own complex reflectivity (amplitude and phase) and with its individual distance from the sensor.

The coherent image formation mechanism coupled with the high phase sensitivity prevents the phase value relative to an individual pixel of a single SAR image from being directly exploitable. On the other hand, as long as the complex reflectivity of the pixel as a whole (i.e. the reflectivity of the elementary scatterers and their differential sensor-target path) does not change in the time span between successive radar acquisitions, it is cancelled out from the interferometric phase. This is the basic assumption for carrying out interferometric measurements and is referred to as absence of decorrelation (or full coherence).

In reality, a residual differential reflectivity term always affects the interferometric phase and is referred to as decorrelation noise. In particular, vegetated areas are often afflicted by temporal decorrelation because of a complex reflectivity varying with time and/or position of the elementary scatterers within the sampling cell (e.g. leaves and small branches of a tree).

Conversely, geometric decorrelation is due to a complex reflectivity that changes with the acquisition geometry (Zebker and Villasenor, 1992). Geometric decorrelation is mainly due to the presence of plural comparable (in terms of the backscattered radiation) scatterers within a single sampling cell. Their differential travel path varies with the acquisition geometry. The principal orbital parameter controlling this effect is the so-called normal baseline B_n, i.e. the projection perpendicular to the LOS direction of the distance of the satellite orbits relative to the two images involved in the interferogram (Fig. 2C).

In summary, the main contributions to the interferometric phase are the following:

- Possible ground deformation Δs, affecting directly the sensor-target travel path. Only the projection of the deformation occurring along the sensor-target LOS (Δs_{LOS}) is appreciated by a SAR system: $\Delta\phi_{def,LOS} = (4\pi/\lambda)\Delta s_{LOS}$. The sensitivity is very high: a LOS displacement of $\lambda/2$ causes a full phase cycle.
- Topographic profiles, in particular the height difference $\Delta q_{1,2}$ between couples of image pixels. The interferometric sensitivity to topography is much lower and is proportional to the normal baseline of the interferogram at hand (the normal baseline is a measure of how different the two orbits are):

$$\Delta\phi_{topo1,2} = \frac{4\pi}{\lambda r_M \sin\theta} B_n \Delta q_{1,2}$$

where $\Delta\phi_{topo1,2}$ is the topographic contribution to the interferometric phase difference between two arbitrary

pixels (named 1 and 2), r_M is the sensor-target distance (approximately 845 km for ERS mid-range), B_n is the normal baseline of the interferogram and $\Delta q_{1,2}$ is the topographic height difference of pixels 1 and 2. The topographic sensitivity of an interferogram is usually quantified by the height of ambiguity (Massonnet and Feigl, 1998; Rosen et al., 2000), i.e. the relative height difference $h_{2\pi}$ between two image pixels that introduces a full phase cycle:

$$h_{2\pi} = \frac{\lambda r_M \sin\theta}{2B_n} \approx (\text{for ERS}) \frac{9350}{B_n} [\text{m}]$$

- Phase noise (both temporal and geometric decorrelation).
- Atmospheric artefacts. Although SAR systems are capable of penetrating the cloud cover, the SAR phase signal is significantly influenced by the atmospheric conditions, in particular by the water vapour distribution in the troposphere (Zebker et al., 1997; Hanssen, 2001). The atmospheric phase distortion (atmospheric phase screen, APS) is strongly correlated in space within each individual SAR image (i.e. it varies smoothly as a function of range and azimuth).
- Possible imprecisions in the orbital data (in particular baseline errors) translate into a further spatially correlated phase term (a low order phase polynomial, Sharroo and Visser, 1998; Hanssen, 2001).

SAR interferometry can be exploited for the generation of topographic maps and 3D terrain models (DEMs) (Zebker and Goldstein, 1986; Zebker et al., 1994a) and for the detection of ground deformation phenomena. The main data processing requirement for a correct DEM reconstruction from interferometric data is phase unwrapping (e.g. Ghiglia and Pritt, 1998) i.e. the retrieval of the unambiguous phase values (with respect to one or more reference points). This is often very difficult because of decorrelation noise and geometric distortion effects which introduce random phase values.

The impact of temporal decorrelation can be reduced by exploiting ERS images acquired in the so-called Tandem mode (images acquired by ERS-1 and ERS-2 with 24 h time span). Moreover, in such a short time interval one can often assume that no significant ground deformation occurred.

Geometric decorrelation has to be carefully dealt with. In fact, the use of higher normal baselines increases the phase sensitivity to the height variations (see formulas introduced before) and, thereby, the achievable vertical precision, but at the same time makes phase unwrapping more difficult. This is because the so-called fringes (i.e. phase cycles) and the corresponding discontinuities ("jumps" from +/− π to −/+ π, very similar to iso-height contours) become denser and the decorrelation noise affecting the interferogram rises.

A useful normalised index of the local signal to noise ratio of the interferometric phase (taking into account both geometric and temporal decorrelation, but not atmospheric distortion) is coherence $|\gamma|$, i.e. the amplitude of the complex correlation coefficient relative to the two images involved in the interferogram:

$$\gamma = \frac{E[\text{MS}^*]}{\sqrt{E[|M|^2] \cdot E[|S|^2]}}$$

where MS* represents the pixel by pixel master-slave conjugated product and $E[\#]$ is statistical expectation. The practical computation of coherence is carried out assuming ergodicity for the interferometric signal and, therefore, estimating $E[\#]$ using all pixels within a (e.g. rectangular) window centred in the image element at hand.

One further problem is the atmospheric signature that can introduce large errors, especially in topography estimates carried out starting from low normal baseline interferograms (Zebker et al., 1997; Hanssen, 2001).

The joint exploitation of more interferograms characterised by different normal baseline values (the so-called multi-baseline approach, Ferretti, 1997; Ferretti et al., 1999a, 2001b) represents an effective way to limit the negative influence of both the decorrelation noise and atmospheric artefacts and to guarantee more reliable phase unwrapping results.

3.2. Production of interferometric digital elevation models (DEMs)

Given the wide-area coverage of SAR and regular repeat-pass of satellites, interferometric DEMs can provide basic topographic information useful especially for regional scale landslide investigations. Indeed, slope angle information is essential for reliable characterization of landslides and assessment of susceptibility of slopes to failure. Currently, topographic maps and digital elevation data derived from photogrammetry are typically used. Alternatively, altimetric data are obtained from Global Positioning System (GPS) or other methods of topographic surveying, or by digitising technical cartography (i.e. indirectly from photogrammetric data).

The quality assessment of a space-borne InSAR DEM is not straightforward. Usually, the vertical standard deviation is provided. Its value can, however, vary significantly, depending mainly on the normal baseline of the interferograms involved, on local decorrelation phenomena, on APS and on the SAR platform used. For areas with high relief topographic features reasonable

figures range from 5–10 to 15–20 m (excluding pixels affected by geometric distortion where phase information can hardly be exploited). Whenever topography is gentle the precision can be finer.

The generation of InSAR DEM appears cost-effective, in particular for wide-area applications (Van der Kooij, 1999). Furthermore, by combining ascending and descending passes (to limit the areas affected by geometric distortion), the topographic detail is comparable with what can be obtained by means of photogrammetry, even though the vertical standard deviation errors are higher.

The main advantages of InSAR are:

- The capability of providing spatially "continuous" data (with exception of low coherence areas) directly in digital format and suitable for ground surface feature extraction.
- The optimal characteristics for covering wide-areas (thousands of square kilometres) at low costs when compared to ground based conventional topographic or GPS surveying and photogrammetric applications.

4. Differential SAR interferometry (DInSAR) for ground deformation detection and monitoring

4.1. Background

InSAR techniques can be applied to detect and measure ground deformation, provided that the topographic phase contribution is removed from a sufficiently long time span interferogram in which interferometric phase surface displacement is recorded. This involves the generation and subtraction of the so-called synthetic interferogram, and leads to Differential SAR interferometry (DInSAR). It can be done either by exploiting an *a priori* DEM (two-pass technique) or by using a Tandem or short temporal baseline "topographic" interferogram (three-pass and four-pass techniques, with or without phase unwrapping of the "topographic" interferogram, Zebker et al., 1994b; Massonnet et al., 1996).

Clearly, any imprecision in the reference DEM translates into a residual topographic phase term whose impact depends on the normal baseline of the interferogram generated for ground deformation mapping. The requirement to keep low the phase noise introduced by geometric decorrelation leads towards the selection of low normal baseline interferograms for performing ground deformation measurements. In theory, differential SAR interferometry has the potential to detect millimetric deformation along the sensor-target LOS. In practice, however, DInSAR performance is heavily reduced by several limiting factors (discussed in the next section), and the quantitative exploitation of the results requires an appropriate modelling and validation of the data quality (e.g. Crosetto et al., 2005).

The DInSAR technique has been successfully used for mapping different ground deformation phenomena. These included volcano dynamics (e.g. Massonnet et al., 1995), co-seismic displacements (e.g. Massonnet et al., 1993), subsidence due to exploitation of ground-water and oil/gas (e.g. Amelung et al., 1999) and mining subsidence (e.g. Carnec and Delacourt, 2000).

4.2. Limitations of conventional differential SAR interferometry in landslide monitoring applications

Despite a few spectacular case studies e.g. the Saint-Etienne-de-Tinée landslide case (Fruneau et al.,

Table 1
Assessment of suitability of ERS data for recognition of geological features through SAR image interpretation and for ground displacement monitoring via SAR interferometry, with reference to slope aspect and inclination (given the average incidence angle, or both the near and far range incidence angles, it is straightforward to adapt the table also to different radar sensors)

Slope aspect	Ascending ERS passes	Descending ERS passes	Notes
Slope facing East	Enhanced range resolution if $\|\alpha\|<67°$ Shadow if $\|\alpha\|>67°$	Foreshortening if $\|\alpha\|<23°$ Layover if $\|\alpha\|>23°$	Only ascending data suitable for SAR interferometry and feature extraction by means of image interpretation. Slopes exceeding 67° are not covered. 1D LOS deformation data.
Slope facing West	Foreshortening if $\|\alpha\|<23°$ Layover if $\|\alpha\|>23°$	Enhanced range resolution if $\|\alpha\|<67°$ Shadow if $\|\alpha\|>67°$	Only descending data suitable for SAR interferometry and feature extraction by means of image interpretation. Slopes exceeding 67° are not covered. 1D LOS deformation data.
Slope facing North or South	–	–	Both ascending and descending data are suitable for interferometry and feature extraction by means of image interpretation. 2D deformation analysis feasible. Low system sensitivity with respect to translational displacements along the North–South direction.

1996, with the results, however, obtained using 3 day revisiting time ERS-1 data gathered in a special acquisition mode in which the sensor was operated only for a couple of months in 1993), and the recognition of some well defined areas suitable for practical applications (e.g. mass movements above the tree line in areas with high topographic relief like the Alps, Rott et al., 1999, 2000; Nagler et al., 2002), DInSAR cannot be currently considered as an operational tool for landslide monitoring.

In order to evaluate the probability of success of a DInSAR analysis aimed at detecting slope instability, the following factors should always be taken into account:

- Geometric decorrelation, which implies that only low normal baseline interferograms can be successfully exploited (e.g. $B_n < 150$–200 m, the exact figure depends on the impact of the other noise sources as well as on the precision of the reference DEM).
- Temporal decorrelation, which is often the main limiting factor whenever the area of interest is (densely) vegetated.
- Atmospheric artefacts, which superimpose on the differential interferogram phase an additional pattern that is often difficult to discriminate from the patterns induced by deformation phenomena (Zebker et al., 1997; Hanssen, 2001). The impact of the so-called atmospheric phase screen (APS) can be reduced in a multi-image framework taking advantage of the fact that APS is uncorrelated in time (i.e. from an acquisition to the following one). This observation leads to interferogram stacking procedures (e.g. Zebker et al., 1997; Sandwell and Price, 1998) and is exploited also within the Permanent Scatterers approach (see Section 4.3).
- Scale constraints, which means that to be effectively appreciated by DInSAR, the unstable area should include at least a few hundreds resolution cells (this is linked to the spatial smoothing effect induced by interferogram filtering). A reasonable figure could be e.g. 10–20 (ground range) times 50–100 (azimuth) sampling cells corresponding to 200–400 m (ground range) times 200–400 m (azimuth).
- The phase measurements are modulo-2π (2π correspond to $\lambda/2$). Theoretically, whenever the LOS projection of the displacement occurred in the time span covered by the interferogram exceeds $\lambda/4$, the resolution of the ambiguity on a pixel by pixel basis is no longer possible (sampling theorem), unless a priori information is available. However, scale constraints imply that with conventional DInSAR one can appreciate only spatially correlated deformation phenomena (e.g. subsidence due to oil/water withdrawal, pre-eruptive inflation, co-seismic deformation). In this case, the problem of solving the phase ambiguity is transferred from time to space. If the spatial gradient of the displacement is not too high (a theoretical upper limit for the deformation gradient along the ERS LOS of 2.9 mm/m is provided by Hanssen, 2001), and the whole area preserves coherence, even deformations of meters (e.g. caused by earthquakes) can be appreciated via 2D spatial phase unwrapping, regardless of the temporal interval they occurred in. Conversely, incoherent ground displacements, i.e. differential deformations of the various scattering elements within single resolution cells (e.g. caused by erosion processes), translate into additional temporal decorrelation. In practice, DInSAR monitoring of incoherent deformation phenomena is usually not feasible.
- The aspect and inclination of the slope, which have direct impact on the feasibility of DInSAR deformation monitoring. The interferometric phase relative to areas affected by significant geometric distortion is, in general, useless. Table 1 summarises the main geometric constraints on the feasibility of an ERS-1/2 DInSAR analysis (the extension to other platforms is straightforward, given the off-nadir looking angle of the sensor).
- DInSAR records the LOS projection of a possibly 3D deformation. As explained in Table 1, on flat terrain and on slopes facing north or south, 2D analysis is feasible by exploiting both ascending and descending passes (an *ad hoc* validation of 2D displacement detection using artificial reflectors is available in Novali et al., 2005). The system has, however, no sensitivity along the sensor orbit. Since both the ERS and RADARSAT orbits are quasi polar, any deformation occurring along the north–south direction originates a very small LOS projection. In general, the LOS projection of deformation (or average deformation rate, i.e. velocity) can be obtained as the scalar product of 3D displacement data, $\underline{d}$ (or velocity, $\underline{v}$) and the so-called sensitivity versor $\underline{u}$ (Massonnet and Feigl, 1998; Colesanti et al., 2003a), whose components highlight the impact of both horizontal (easting and northing) and vertical phenomena on the LOS measurement carried out by the SAR system:

$$d_{LOS} = \underline{d} \cdot \underline{u} = \begin{bmatrix} d_{\text{East}} \\ d_{\text{North}} \\ d_{\text{Zenith}} \end{bmatrix} \cdot \begin{bmatrix} u_{\text{East}} \\ u_{\text{North}} \\ u_{\text{Zenith}} \end{bmatrix},$$

$$v_{LOS} = \underline{v} \cdot \underline{u} = \begin{bmatrix} v_{\text{East}} \\ v_{\text{North}} \\ v_{\text{Zenith}} \end{bmatrix} \cdot \begin{bmatrix} u_{\text{East}} \\ u_{\text{North}} \\ u_{\text{Zenith}} \end{bmatrix}$$

$$\begin{bmatrix} u_{\text{East}} \\ u_{\text{North}} \\ u_{\text{Zenith}} \end{bmatrix} \approx \begin{bmatrix} 0.38 \\ -0.08 \\ 0.92 \end{bmatrix}$$

where the values provided for the components of $\underline{u}$ are referred approximately to the centre of a descending ERS scene (the components vary slowly, mainly as a function of the slant range co-ordinate). Since $\underline{u}$ points from the target to the sensor, a LOS target motion towards the satellite is registered as a positive displacement (or velocity). Furthermore, each component of the sensitivity versor highlights the corresponding quota of deformation that is mapped along LOS and detected by the SAR sensor (e.g. about 38% of possible east–west deformation is recorded by ERS DInSAR data).

In landslide monitoring, the following two movement components play a particular role: the downslope direction (in case of movements subparallel to the slope), and the vertical direction (in case of predominantly rotational movements). This implies that DInSAR displacement data can be fully exploited and correctly interpreted only when other sources of information (mainly ground truth) allow assessing to what extent the deformation is rotational and/or translational.

4.3. Permanent Scatterers (PS) technique

Although this paper is focused on the Permanent Scatterers (PS) technique, for the sake of completeness, it is considered worthwhile to provide a brief chronological overview of the recently developed advanced interferometry techniques. The core purpose is to provide references for the reader interested in other multi-image DInSAR approaches.

As highlighted in the previous section, while studying the effect of atmospheric artefacts on SAR interferograms, Zebker et al. (1997) suggested that, aiming at ground deformation monitoring, such artefacts could be reduced by averaging independent interferograms (this, of course, corresponds to exploiting the temporal incorrelation of the atmospheric phase contribution). This approach was further developed into the so-called interferogram stacking technique by Sandwell and Price (1998). A similar idea underlies also the wavelet domain weighted combination foreseen within the multi-baseline DEM reconstruction proposed by Ferretti (1997) and Ferretti et al. (1999a, 2001b).

Meanwhile, the PS technique was being developed at Politecnico di Milano. The first results were published in 1999 (Ferretti et al., 1999b). Later, other research groups developed more or less similar PS processing tools and reported relevant results (Refice et al., 2001; Kampes and Adam, 2003; Ketelaar and Hanssen, 2003; Bovenga et al., 2004; Hooper et al., 2004).

In 2001 a different family of multi-image SAR interferometry techniques was presented to the public. The core idea is the generation of several sets of low baseline interferograms using different master images. To combine measurements that are not structurally self consistent (since there is not a single master shared by all interferograms), a single value decomposition framework (Berardino et al., 2001, 2002; Lanari et al., 2004) or a minimum least squares approach (Usai, 2002, 2003; Le Mouélic et al., 2003) were adopted.

In 2001 also, Costantini et al. (2001) defined a multi-image interferometric approach generalising in three dimensions (i.e. space plus time) the phase unwrapping problem (Costantini et al., 2001, 2002).

In 2003, Werner et al. (2003a), Van der Kooij (2003) and Duro et al. (2003) presented results obtained respectively via the "interferometric point target analysis", the "coherent target analysis" and the "stable point network analysis". The details of these approaches are still unknown to us, but it seems they resemble rather closely the PS approach.

A detailed description of the PS technique, the first validating experiments and a formal precision assessment can be found respectively in Ferretti et al. (2000a, 2001a) and in Colesanti et al. (2003a,b). Here we offer some background information and address limits and potential of the technique. We also show how several factors that reduce the practical applicability of conventional DInSAR to landslide monitoring can be overcome by using the Permanent Scatterers technique.

Basic principles of the PS approach are:

- The scattering mechanism of a certain amount of image pixels is dominated by a single point-wise element (i.e. much smaller than the image pixel), whose contribution overwhelms the coherent sum of all other scattering elements present within the same sampling cell. This implies that the interferometric phase of these privileged pixels is only slightly affected by geometric decorrelation. Moreover, as long as these dominant scatterers correspond to objects whose reflectivity does not vary in time (in particular portions of man-made structures and bare rock exposures), temporal decorrelation is also negligible.
- The radar targets, only slightly affected by decorrelation, allow creating a set of (N) differential interferograms all referred to a unique master, regardless of temporal (even year long time spans) and normal baseline values (in general for ERS B_n values range between ±1200 m). To this end the (N+1) available SAR images need to be re-sampled (co-registered) on the grid of the unique master image.

- The various interferometric phase contributions (residual topography due to the limited precision of the DEM used for generating the differential interferograms, APS, orbital inaccuracies, possible ground deformation and noise) are then precisely separated at individual PS in the framework of a joint time–space — normal baseline analysis exploiting their different spectral behaviour.
- Sampling cells that are likely to behave as Permanent Scatterers can be identified in advance by means of a pixel by pixel statistical analysis of the amplitudes of the $N+1$ available SAR images (Ferretti et al., 2001a).
- Permanent Scatterers form a sparse grid whose spatial density can even exceed 500 PS/km^2 in urban areas. It is not possible to provide a generally valid figure for the PS density in rural or low urbanisation areas, mainly because the number of "natural" PS (corresponding to exposed rocks) seems to vary strongly in relation to local lithology and morphology (Dehls et al., 2002). Recent tests showed natural PS densities varying from 0–10, 20–50 up to 200 PS/km^2 (the actual PS density depends also on the threshold set on phase stability to identify PS). The retrieval of empirical laws relating the expected PS density to local geologic settings is of much interest as this would help to predict the success probability and the amount of output data that can be obtained by means of a PS analysis.
- A sufficient number of SAR images must be available to perform a PS analysis (~15–20 ERS images, Colesanti et al., 2003a,b) and the PS spatial density has to be high enough (at least 5 PS/km^2). This last requirement is fundamental for isolating and removing the atmospheric phase term by exploiting jointly its spatial correlation and temporal uncorrelation.

Permanent Scatterers can be thought of as benchmarks of a high density geodetic network. For each PS the output products of the analysis are (Colesanti et al., 2003a,b):

- Full displacement LOS time series. The precision (in terms of standard deviation) of each single measurement ranges between 1 and 3.5 mm. As in all DInSAR applications, deformation data are relative both in time and space. In time all data are referred to the unique master image. In space data are relative to a reference PS supposed motionless. Average LOS deformation rates can be determined with submillimetric precision (typical values range from 0.1 to 1 mm/yr).
- High precision (standard deviation ~1 m) elevation estimate of PS (the phase discrimination carried out at single PS allows estimating the residual topographic term due to the limited precision of the reference DEM used for generating the differential interferograms).

The PS approach allows overcoming several limiting factors affecting DInSAR measurements:

- Extremely reduced impact of decorrelation noise. As long as a sufficient spatial density of individual PS is available, deformation analyses can be carried out in low coherence areas, thereby exploiting isolated PS even if fully surrounded by incoherent pixels (e.g. single building or outcrop in a forest area). This is, indeed, a major advantage with respect to conventional interferometry, especially for slope instability and landslide monitoring applications, where the capability of providing measurements also in a vegetated environment is often required.
- The atmospheric artefacts are estimated and removed. Combined with the low amount of decorrelation, this allows reaching the precision of deformation measurements very close to its theoretical limit (around 1 mm for C band sensors like ERS and RADARSAT).
- Point-wise measurements enable to characterise local deformation effects; for instance movements affecting individual buildings whose surroundings are perfectly stable can be detected (Ferretti et al., 2000b; Colesanti et al., 2001).
- Starting from precise elevation data, high precision geocoding of PS positions is possible. Permanent Scatterers can be mapped on the corresponding man-made structures or natural targets, e.g. in a GIS environment (Colesanti et al., 2001) or on high resolution optical imagery.
- Each result (LOS displacement time series, average LOS deformation rate and height of every PS) can easily be provided with a precision figure (standard deviation of the estimate, see Colesanti et al., 2003b for details). A correct exploitation and understanding of the results by users not having a direct expertise in interferometry is thereby facilitated.

Moreover, a significant advantage of the PS approach and, in general, of DInSAR with respect to in situ measurements (e.g. optical levelling and GPS surveys) is the possibility to investigate a posteriori past deformation phenomena. To this end, the ESA ERS archive gathering data since 1991/92 is of incomparable value. The feasibility of PS analyses involving jointly ERS-1/2 and ENVISAT data has been proven (Arrigoni et al., 2003; Duro et al., 2003), thereby ensuring the continuation of the ESA archive for the next years.

On the other hand, some drawbacks of DInSAR techniques still limit the performance of a PS analysis. While listing them, we provide hints on possible ways to tackle such limiting factors, thereby pointing to some of

the currently most important research topics in PS InSAR interferometry and giving the reader an idea of the main achievements that can be envisaged for the near future.

●As already mentioned, displacement data represent the 1D LOS projection of a deformation that can actually occur in all three dimensions. This limit can be at least partially circumvented merging results from PS analyses carried out on distinct data sets e.g. parallel tracks and ascending–descending data sets acquired by the same sensor as well as datasets from different platforms (Rocca, 2003; Novali et al., 2005). Of course, this requires mapping independent PS grids on each other, taking into account that, most likely, different parts of the same object (e.g. building) behave as PS for different acquisition geometries and/or sensors (Colesanti et al., 2002, 2003c).

●The ambiguity of phase measurements implies the impossibility to track correctly and unambiguously a single PS LOS deformation exceeding $\lambda/4$ (=1.4 cm for ERS) within one revisiting time interval (35 days for ERS), i.e. approximately 14.5 cm/yr. In practice it is extremely difficult to detect LOS displacement rates exceeding 8–10 cm/yr. This limit can be relaxed in two ways:

○ (a.) Exploiting the possible spatial correlation of the ground deformation phenomenon at hand (cf. previous section on conventional DInSAR), e.g. via modelling. This allows one to transform the 1D problem of resolving the phase ambiguity in time within the time series of a single PS into a 2D (spatial) or 3D (spatio-temporal, Costantini et al., 2001, 2002) phase unwrapping problem (cf. also Ferretti et al., 2000a), and leads to upper LOS velocity limits close to the ones of conventional DInSAR. The issue has, however, to be dealt very carefully with. As a matter of fact, imposing a deformation model can prevent the PS analysis from correctly detecting very localised small-area phenomena not reflected by the model, thereby heavily penalising one of the most advantageous features of the PS approach, i.e. the single building monitoring capability.

○ (b.) Carrying out plural PS analyses involving SAR data acquired at different frequencies. For instance L-band JERS data have $\lambda/4=5.9$ cm and a revisiting time of 44 days. This results in a LOS velocity limit larger than 45 cm/yr. Of course this implies also that the precision of JERS PS measurements is about 4 time worse than the one of ERS PS. By carrying out a PS analysis on both ERS and JERS data sets and merging the (geo-coded) results one can profit from the reduced JERS sensitivity to ambiguity problems and from the higher precision of ERS PS measurements. The issue is of particular interest since the L-band data from a new space-borne sensor, ALOS, should become available in 2006. It is worth remarking that PS results obtained from JERS data have already been reported (Giordani and Panzeri, 2003; Werner et al., 2003b; Daito et al., 2003).

●Limited versatility in terms of (a.) positioning of the measurement points and (b.) revisiting time. Both parameters (a.) and (b.) cannot be optimised freely as degrees of freedom while planning a PS analysis. Nevertheless, in areas characterised by the presence of important infrastructures, passive metallic (corner, planar or dihedral) reflectors can be deployed *ad hoc* so as to create additional "artificial" PS (Novali et al., 2005). Clearly, in this case additional costs are involved and the SAR historical imagery cannot be exploited. The constraint on the revisiting time can be, once more, partially relaxed merging results from PS analyses carried out on distinct data sets (from the same or from different sensors).

●Finally, it is still difficult to anticipate the PS density in rural areas without carrying out at least several processing steps on a significant number (>15–20) of SAR images. In this respect, it is worth mentioning an ongoing research activity aimed at the classification of individual PS into different typologies (e.g. mirror-like or trihedral, dihedral, pole-like, resonating structure

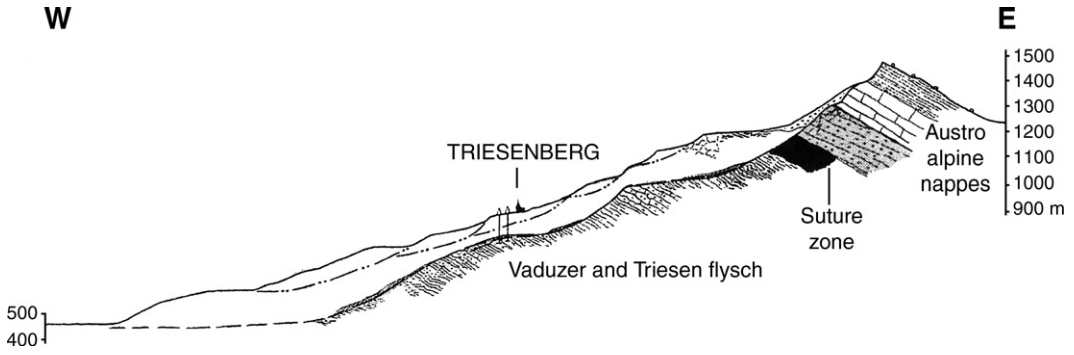

Fig. 4. Cross section of the Triesenberg–Triesen landslide (modified after Allemann, 2002). Vertical scale=horizontal scale.

etc.). This is achieved combining data acquired from different geometries, polarisations and platforms. Remarkable results of PS classification in urban areas have already been reported (Ferretti et al., 2005; Perissin et al., 2005). The nature of PS not corresponding to man-made structures can be investigated in depth by extending the analysis to rural areas.

5. Example of landslide investigation using PS technique

To illustrate the practical applicability of the PS interferometry we present the outcomes of a study exploiting a nine-year set of radar satellite data for investigating the Triesenberg–Triesen landslide. We expand upon the initial work of Colesanti and Wasowski (2004) by providing more detailed analysis of the SAR data and discussing more in depth the implications of the PS displacement results for the landslide assessment.

5.1. Physical and geological setting

The area studied is located in the Liechtenstein Alps, a few kilometres south of the country's capital Vaduz (Fig. 1). The Triesenberg–Triesen landslide (Allemann, 2002) occupies the west facing slopes of the Rhine river valley characterised by high local relief (over 1000 m). The two main towns affected by landsliding are Triesen and Triesenberg, located respectively at about 500 and 900 m a.s.l.

The area is situated in the western-most part of the Eastern Alps, near the main Alpine suture zone developed along the Austroalpine/Penninic boundary. The local tectono-stratigraphic relations in the landslide area are shown in Fig. 4. The bedrock of the middle–lower slopes is constituted by Late Cretaceous and Late Cretaceous–Earliest Tertiary flysch units known as Vaduzer and Triesen Flysch (Allemann, 2002). The flysch beds are characterised by counter-slope dips, locally exceeding 40°. The upper slopes contain deformed units arranged in tectonic nappes. A variety of rocks is present including Perm-Trias age sandstones, undifferentiated flysch and breccias, and Late Cretaceous flysch and chalks. The bedding is irregular, but counter-slope dips predominate.

A vast hillslope area is mantled by Quaternary age superficial deposits, which include also considerable amounts of coarse materials of rock fall and rock slide origin. Talus materials are present in the upper slope area, at the base of steep rock scarps. Moraine deposits crop out extensively along the middle slopes of the

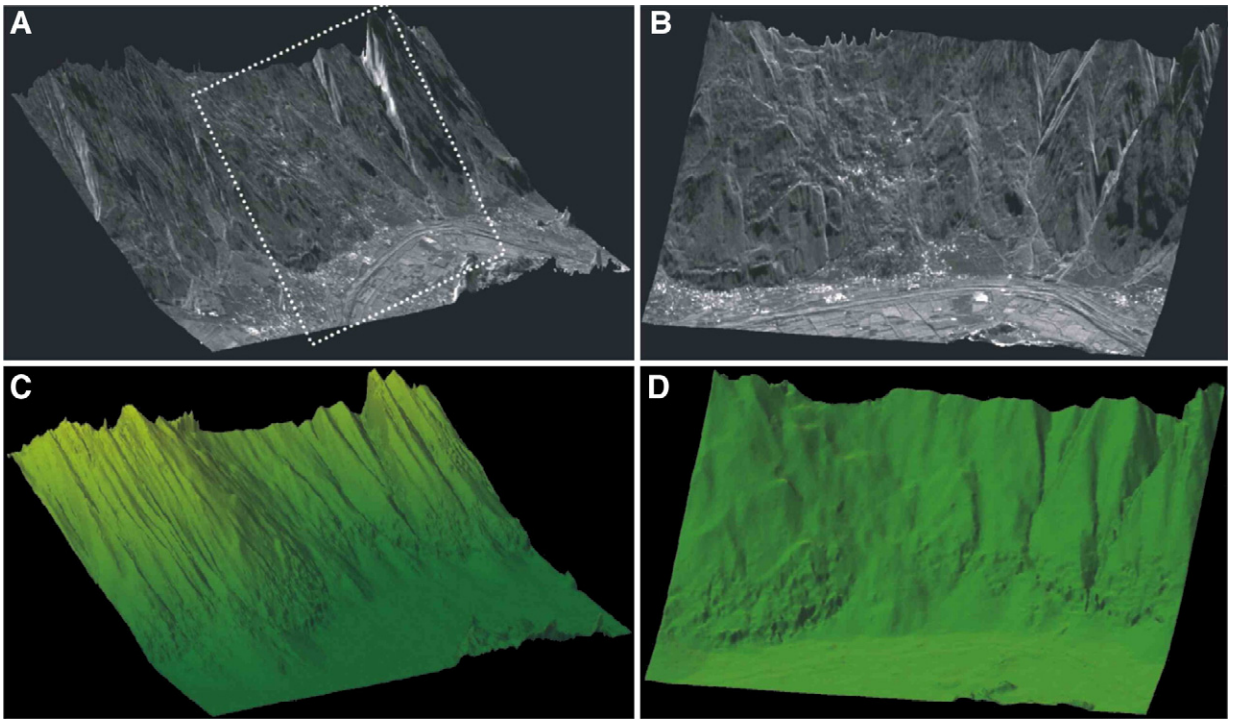

Fig. 5. SAR multi-image reflectivity maps (A, B) and the interferometric digital elevation models (DEMs) (C, D) of the west facing Rhine River valley slopes and the Triesenberg–Triesen landslide. The white-dotted rectangle marks a close-up of the area affected by the landslide (shown in B, D). The vertical axis is exaggerated for visualisation purposes.

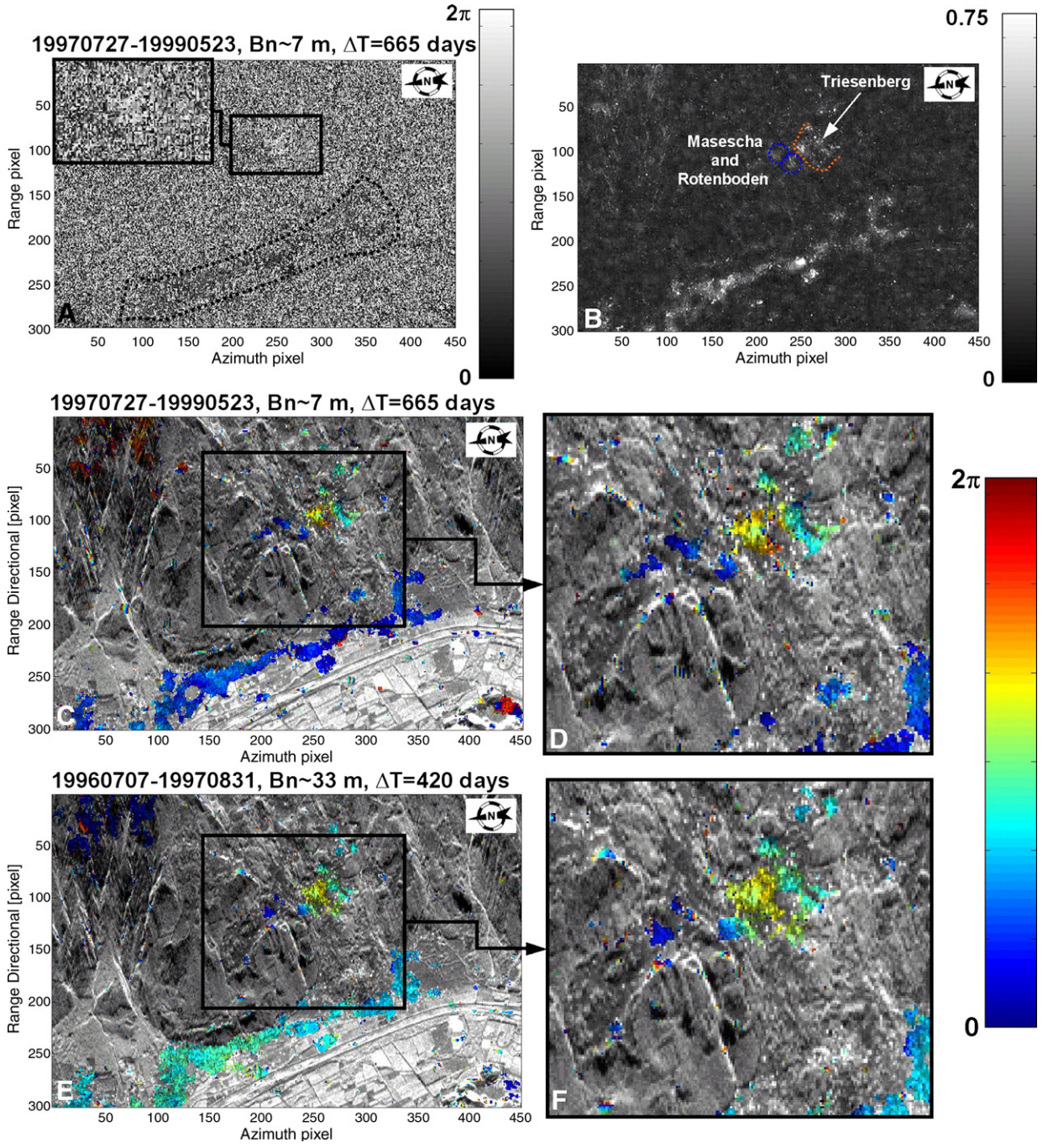

Fig. 6. Conventional DInSAR results for the study area. (A) Interferometric phase (interferogram filtered via simple 5×5 boxcar averaging) with a close up on the area of Triesenberg (black rectangle). The dotted line marks the urbanised part of the Rhine valley characterised by a good SNR on the interferometric phases, i.e. by a high coherence. (B) Coherence relative to the interferogram in (A); the blue and red dotted lines identify respectively the position of Masescha/Rotenboden and Triesenberg where a reasonable coherence is preserved as well. (C, D) Interferometric phase relative to the interferogram 23 May 1999–27 July 1997 (B_n=7 m, time span=665 days). The interferogram is filtered as in Ferretti (1997), and coherence masked, i.e. only pixels with coherence above a threshold is displayed. (E, F) Coherence masked filtered (Ferretti, 1997) interferometric phase relative to the interferogram 31 August 1997–7 July 1996 (B_n=33 m, time span=420 days). A local gradient of more than half a phase cycle in the area of Triesenberg (blue to yellow-light orange in image D) suggests the occurrence of roughly 2 cm LOS deformation in approximately two years (July 1997–May 1999). Interferogram (F) provides a further evidence of ongoing deformation, with a similar LOS rate, in the time span July 1996–August 1997.

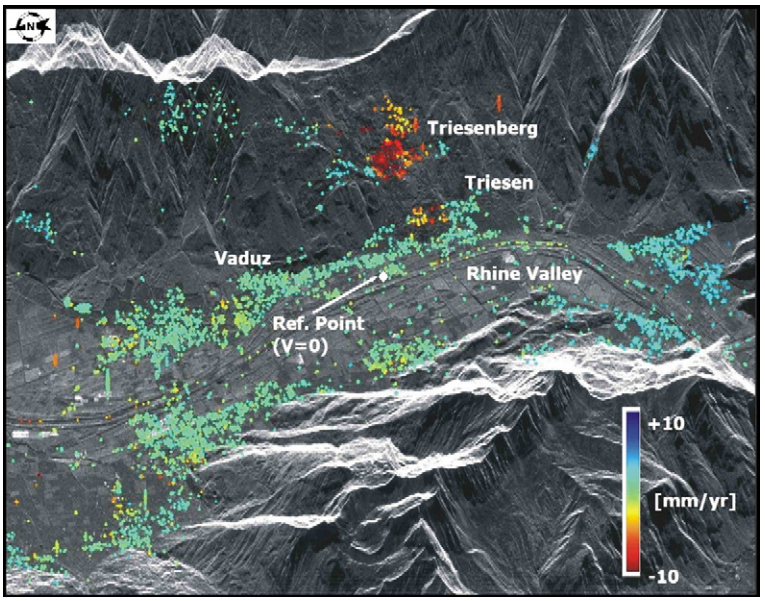

Fig. 7. SAR multi-image reflectivity map of the study area showing the distribution and average Line Of Sight (LOS) displacement rates of Permanent Scatterers (PS) indicated by colour dots. The images are in SAR co-ordinates, with 4 times oversampling applied along range. LOS velocity has been saturated at ±10 mm/yr for visualisation purposes only. Note location of the reference point assumed motionless (velocity $v=0$).

valley. Finally, large alluvial fans are present at the slope base near the northern and southern lateral margins of the Triesenberg–Triesen landslide.

5.2. The Triesenberg–Triesen landslide

The Triesenberg–Triesen hillslope is covered by a large landslide (Figs. 1, 4), which has an area of approximately 4.2 km^2 and estimated volume of 500 million cubic meters (Allemann, 2002). The borehole data indicate the maximum depth is about 80 m. The origin of the landslide may date back to the retreat of the Rhine valley glacier, which took place over 10,000 years ago. Today the toe of the landslide complex is distant a few hundred meters from the Rhine River and appears unaffected by fluvial erosion.

The overall landslide slope is between 18.5° and 22°, but there are several local slope breaks (Fig. 4). Two main streams follow lateral flanks of the landslide, whereas the groundwater flow pattern within the slide mass is not known. There appear to be several shallower landslide movements superimposed on the main slide mass (Fig. 4) and this adds some complexity to the mechanism of motion. Nevertheless, the inferred basal slip geometry indicates that the movements are predominantly translational (Fig. 4).

There is ample evidence of the recent and ongoing activity of the landslide. This include the recurring damage to the roads and to several buildings, especially those located in Triesenberg. Furthermore, surface movements were measured during the topographic campaigns in the 1980's and the GPS surveys in 1990's (Frommelt, 1996). The inclinometer monitoring demonstrated the presence of deformations occurring at depths varying from several to about 20 m (GEOTEST AG, 1997). All the ground control data indicate the occurrence of displacements with the average velocity between 1 and 4 cm/yr.

5.3. Interferometric analysis

The PS analysis was conducted as a "blind experiment", i.e. without any auxiliary data, apart from the information regarding the geographical co-ordinates and the predominant facing direction of the hillslope of interest. Considering the size of the hillslope, the investigation was carried out on a larger area (16×16 km^2) centred on the Triesenberg–Triesen landslide. A total of 38 descending mode ERS images covering the time span August 1992–August 2001 were used for this study. The landslide slope faces approximately west, which makes the exploitation of descending mode data ideal for interferometric purposes (Table 1). Nevertheless, geometric distortion effects can be identified on the multi-image reflectivity maps of the test area (Figs. 1, 3B). In particular, layover and foreshortening affect the slopes facing east and local shadowing phenomena are present on steep slopes (>67°) facing west.

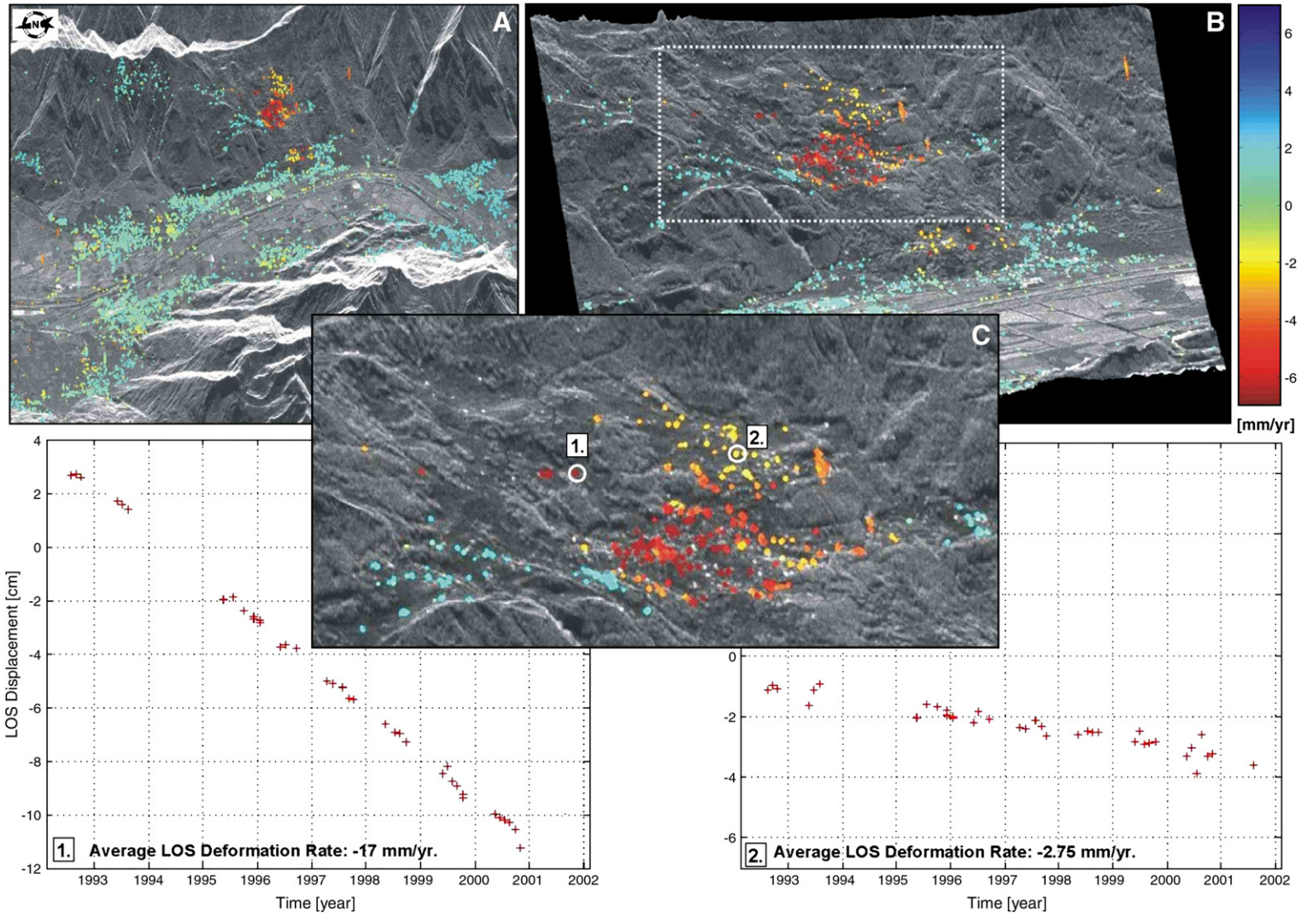

Fig. 8. Radar images of the Triesenberg–Triesen landslide site showing positions and average Line Of Sight (LOS) displacement rates of the Permanent Scatterers (marked by colour dots). A) SAR image showing the landslide location within the Rhine river valley; white square near the centre of the image marks the reference PS supposed motionless; B) SAR image showing the landslide slope; white dotted rectangle indicates the area represented in C); C) SAR image showing locations of two representative PS located on the landslide (marked 1., 2.). The images are in SAR co-ordinates, with 4 times oversampling applied along range. The pixel size amounts, therefore, to 4 m in azimuth and 3 to 5 m (depending on the local slope) in ground range. LOS velocity has been saturated at ±7 mm/yr for visualisation purposes only. The graphs show LOS displacement time series of the PS 1 and 2.

Fig. 9. A 1997 orthorectified aerial photo (original scale 1:5000) of a portion of the Triesenberg–Triesen landslide upslope the town of Triesenberg showing positions of the Permanent Scatterers (color dots) and their Line Of Sight (LOS) displacement rates. White circle indicates the location of PS 1 shown in Fig. 8C. Note ground surface deformations characterising the down slope area to the left of PS 1 (red dot); its surface expression resembles that of an elongated (about 270 m) landslide-like feature; road is approximately 7.5 m wide.

A multi-baseline InSAR DEM (Ferretti et al., 1999a, 2001b) was reconstructed by exploiting jointly three Tandem pairs: 9–10 December 1995, 13–14 January 1996, 9–10 October 1999 (Fig. 5). The DEM helps to appreciate the overall topographic setting of the area and also highlights some geomorphologic features useful for a preliminary assessment of mass movement and erosion processes in the valley (e.g. slope breaks, steep scarps, alluvial and/or debris fans, stream incisions).

5.3.1. Results of conventional differential interferometry analysis

The application of conventional DInSAR approach to the Triesenberg–Triesen landslide produced results that are not fully satisfying. Only low normal baseline interferograms were generated (characterised by the absence of geometric decorrelation and residual topographic phase terms). Fig. 6 shows the interferograms of 23 May 1999 (master)–27 July 1997 (B_n=7 m, time span=665 days) and of 31 August 1997 (master)–7 July 1996 (B_n=33 m, time span 420 days). One can appreciate good coherence i.e. a reasonable signal to noise ratio (SNR) on interferometric phase data at the bottom of the Rhine Valley. In the area of Triesenberg some coherence is also preserved (Fig. 6B). Using the very effective interferogram filtering technique discussed in Ferretti (1997) and masking the interferograms with the respective coherence maps (i.e. representing the interferograms only where the SNR is reasonable) greatly enhances the legibility of the interferometric phases (cf. Fig. 6C, D and Fig. 6A). In the interferogram covering the time span July 1997–May 1999, a phase variation of approximately 4 radians (transition from blue (0 rad) to yellow-light orange (4 rad), corresponding to about 1.5 to 2 cm LOS deformation) can be appreciated (Fig. 6D) moving from Masescha and Rotenboden to and across Triesenberg. A slightly lower amount of LOS deformation is visible also in the second interferogram (Fig. 6F), which covers a shorter time span. An interferogram involving the same two SAR images (of 31 August 1997 and 7 July 1996) is included also in Nagler (2002) and shows a similar phase pattern.

The above results are, however, not fully satisfactory since:

- It is unclear whether the area affected by deformation extends up- and down-hill outside the town centre of Triesenberg.
- Nothing can be stated with reasonable confidence about the town of Triesen. The first interferogram (July 1997–May 1999) does not highlight any deformation (but is the amount of LOS deformation simply too small?), whereas in the second interferogram coherence is not even preserved.
- The first interferogram seems to suggest possible localised differential deformations within the landslide body (local gradients in the interferometric phase can be guessed), but this cannot be confirmed by the second interferogram.

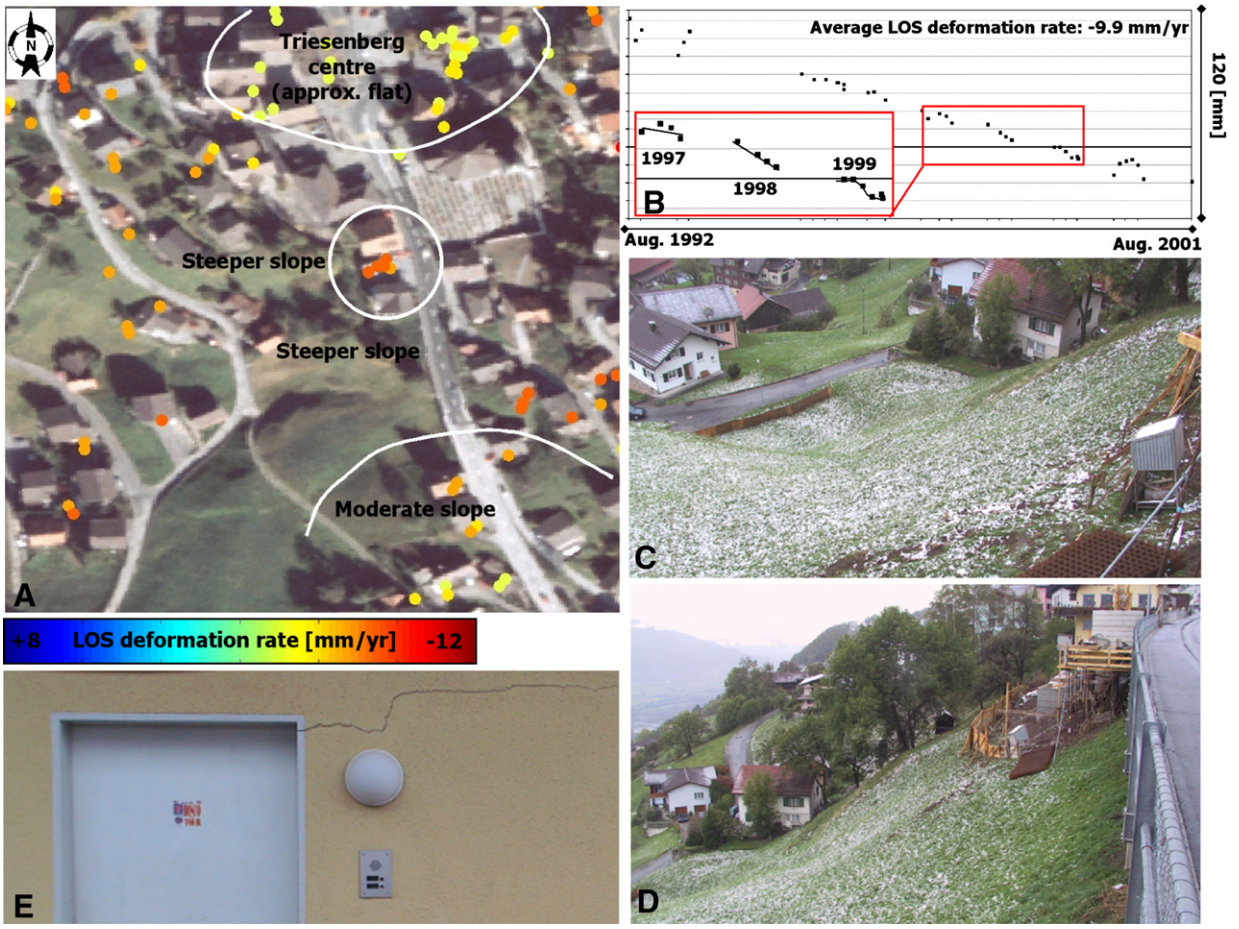

Fig. 10. Line Of Sight (LOS) time series and site conditions of a relatively high-velocity Permanent Scatterer (PS) from the centre of Triesenberg. A) PS position and LOS velocities superimposed on a 1997 orthorectified aerial photo (original scale 1:5000). The PS on the locally steeper slopes just south and west of the centre of Triesenberg show higher average LOS deformation rates (−7 to −11 mm/yr versus −4 to −5 mm/yr in the town centre). B) LOS deformation time series of the PS marked by the white circle in A. The close-up (April 1997–October 1999, overall LOS deformation: 2.5 cm) highlights different average deformation rates in years 1997, 1998 and 1999. In 1999 the evolution is non-uniform in time: the whole displacement (7–8 mm) occurs in two months. C) and D) Two 2003 photographs showing top and side view of the steep slope, whose uppermost part is the site of the PS marked by the white circle in A. Note ground surface morphology indicative of a local slope movement and the ongoing (as of 2003) stabilisation works. E) Cracks on a building corresponding to the PS shown in A and B (and visible also in the upper right corner of photograph D).

In practice it is reasonable to claim the detection of a LOS movement in the order of 1 cm/yr affecting an area of roughly 600×600 m^2 corresponding more or less to the centre of Triesenberg. The reason behind the limited conclusions that can be drawn from the analysis of the two interferograms is likely related to the fact that many individual phase stable pixels (mainly houses) are surrounded by cells corresponding to vegetated areas affected by temporal decorrelation.

5.3.2. Results of PS analysis

The difficulties encountered with the DInSAR approach were overcome by applying the PS technique. The analysis resulted in the identification of around 7500 PS in

Fig. 11. Slope dependent variation in Permanent Scatterers (PS) Line Of Sight (LOS) velocities at Triesenberg: A) 1:5000 scale topographic map of the town centre area. Continuous thick black lines are 5 m contour intervals and dashed black line marks the trace of profiles shown in Fig. 11B,C. Average LOS displacement velocities of PS, indicated by colour dots, range from about 4 to over 10 mm/yr (corresponding to a change from light yellow to red colours); B) Variation in average LOS PS velocities (in mm/yr) along the down slope longitudinal profile, parallel to the presumed direction of landslide movement (from ENE to WSW); C) Longitudinal slope profile. Note that the nearly flat portion of the profile corresponding to the town's centre is characterised by the lowest PS velocities (around 4–5 mm/yr).

the 16×16 km^2 area (average density of 30 PS/km^2). Fig. 7 shows that the PS are mainly distributed along the Rhine valley bottom, where the density of man-made structures is the highest. Despite the geometric distortion, some PS were also identified on the slopes facing east. As anticipated, many stable radar targets useful for

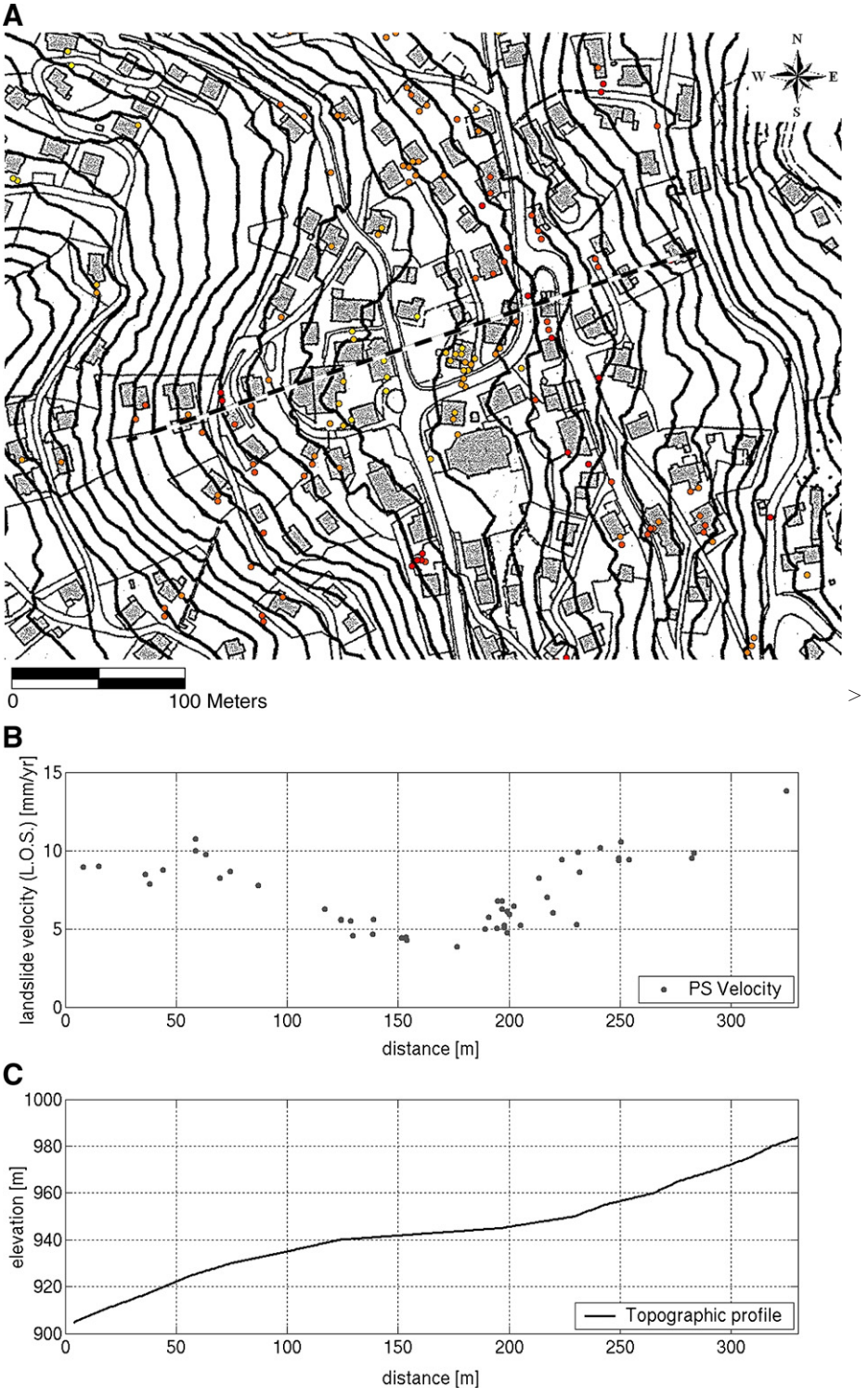

monitoring were found on the west facing slopes. The PS coincide mainly with buildings and, secondarily, with structures made of stone, cement and metal (e.g. perimetral or retaining walls, guard rails, poles). Some PS targets correspond also to bare rock outcrops.

The Triesenberg–Triesen area affected by the landslide is characterised by a high PS density in relation to the enhanced resolution on west facing hillslopes. Under such conditions, each PS is expected to dominate on the coherent sum of the contributions relative to other elementary scatterers disposed in a smaller sampling cell than in the case of flat terrain. Using an interferometric DEM derived directly from the ERS data we estimate an average slope inclination of around 22° with respect to flat terrain. Then, considering that the slope faces approximately west, we obtain a qualitative value of 11–12 m for the ground range sampling step (to be compared with the 20 m relative to flat terrain).

The area analysed is approximately in the centre of a full ERS scene (Track: 480, Frame: 2655, Mode: descending) and the local components of the sensitivity versor u are:

$$\begin{bmatrix} u_{\mathrm{East}} \\ u_{\mathrm{North}} \\ u_{\mathrm{Zenith}} \end{bmatrix} = \begin{bmatrix} 0.375 \\ -0.082 \\ 0.923 \end{bmatrix}$$

Fig. 7 shows the locations and average LOS deformation rates of PS. The boundaries of the deforming area can be identified by following a sharp velocity gradient existing between the PS located within the landslide body and stable points present in the surrounding area. The data indicate that the area affected by the landslide includes the towns of Triesenberg and Triesen, and nearly reaches the bottom of the valley.

Around 450 PS were identified within the 1.7×2.2 km^2 area affected by most significant displacements, i.e. where V_{LOS} systematically exceeds −2mm/yr (n.b. the negative sign stands for displacements away from the radar sensor, down slope in our case). Although the average PS density is around 120 PS/km^2, in some steep slope areas covered by trees, notably between Triesenberg and Triesen, PS are lacking.

5.3.3. Interpretation of the PS results

The PS LOS displacement rates vary from 0 to −20 mm/yr, which, assuming the occurrence of only translational down slope movements would correspond to actual velocities between 0 and ~ −30 mm/yr. Thus, a simple distinction between the stable and unstable areas can readily be made by examining the distribution of the PS and their velocities (Fig. 7). Keeping in mind that for the portions of the hillslope without suitable radar targets no information was obtained, the PS results show that:

- the great majority (over 95%) of moving PS fall within the Triesenberg–Triesen landslide;
- the two main zones with moving PS coincide with the urban and peri-urban areas of Triesenberg and the northern periphery of Triesen;
- the majority of the slopes surrounding the landslide have higher inclinations (over 22°), but, except for one site, appears unaffected by deformations;
- the alluvial fans present along the Rhine valley slope base and the river valley bottom appear stable.

Additional information can be obtained by examining PS and their LOS velocities on a more detailed scale. The graphs in Fig. 8 show also the LOS displacement time series of two PS (PS1 and PS2) located in the Triesenberg area. The evolution of PS1 situated upslope the Triesenberg centre seem nearly time-uniform, except for the year 1996, when a period characterised by the lack of apparent movement was detected. The standard deviation on each measurement, estimated according to Colesanti et al. (2003b), is within 2 mm. The time series relative to PS2, situated at few hundred meters distance from PS1, shows a much slower displacement velocity and is slightly more noisy ($\sigma \approx 2.2$ mm). PS2 belongs to the upper part of the landslide, where the deformation rates of PS are typically within a few mm/yr. The reasons for this are not certain, but it might be in part linked to the presence of relatively lower slope inclinations (~ 14–15°) in that area.

The interpretation of the PS motion data can be greatly facilitated by overlying their geo-coded distribution on a detailed scale orthophoto of the area of interest. For instance, using the orthophoto shown in Fig. 9, it is possible to identify the exact location of PS1 and to obtain some preliminary information on the site via photo-interpretation. In particular, PS1 results to be situated on the down slope side of the local road. It seems significant that a few other PS exhibiting similar, relatively high LOS velocities (exceeding −15 mm/yr) are also located on the down side of the road tract. Furthermore, the orthophoto shows that the ground surface below PS1 appears more deformed with respect to the surrounding area and it seems to form an elongated landslide-like feature that extends down slope towards the town of Triesenberg. This steep area (20–23° slope) has been known for slope instability problems and the deformations have already been monitored there in the past using GPS and inclinometers (Frommelt, 1996, GEOTEST AG, 1997). The site visit in 2003 revealed the presence of damaged retaining walls as well as of deformed and cracked road pavement.

Similarly, as shown in Fig. 10, with the aid of the orthophoto it is possible to visualise the distribution of the single PS in the urban area of Triesenberg and gather some preliminary information on the local site conditions. Indeed, the orthophoto with the plotted distribution of the geo-coded PS has been found very useful in the subsequent in situ location and more detailed examination of the PS site conditions, in light of their varying displacement velocities (Fig. 10).

The PS monitoring results can be compared with the ground surveying that indicated the general displacement rates for the Triesenberg–Triesen landslide between 1 and 4 cm/yr. The average deformation rate along the slope v_{Slope} (responsible for the LOS velocity v_{LOS} measured by means of the PS approach) is retrieved by taking account of the components of the sensitivity versor u):

$$\underline{v} \cdot \underline{u} = v_{\mathrm{LOS}}$$

For the sake of simplicity we assume that the slope faces exactly west and that the deformation is translational, i.e. parallel to the slope. Given that the slope has an average inclination $|\alpha|=22°$, the 3D velocity vector $\underline{v}$ (cf. Fig. 2D):

$$\underline{v} = \begin{bmatrix} -v_{\mathrm{Slope}}\cos|\alpha| \\ 0 \\ -v_{\mathrm{Slope}}\sin|\alpha| \end{bmatrix}$$

where v_{Slope} represents the velocity along the slope. Consequently:

$$v_{\mathrm{LOS}} = \underline{v} \cdot \underline{u} = -(v_{\mathrm{Slope}} u_{\mathrm{East}} \cos|\alpha| + v_{\mathrm{Slope}} u_{\mathrm{Zenith}} \sin|\alpha|)$$

and

$$v_{\mathrm{Slope}} = -\frac{v_{\mathrm{LOS}}}{u_{\mathrm{East}}\cos|\alpha| + u_{\mathrm{Zenith}}\sin|\alpha|} \approx -\frac{v_{\mathrm{LOS}}}{0.7} = -1.43 \cdot v_{\mathrm{LOS}}$$

Therefore, the average displacement rates along the slope are expected to range between 2.8 and 28 mm/yr, which is comparable with the deformation rate detected by means of ground surveys.

As a further example, the scaling factor necessary to obtain the translational deformation (from its LOS measure relative to ERS descending mode data) along a 22° inclined north facing slope would amount to around 2.4 (mainly because the system has a low sensitivity to horizontal displacement towards north). Clearly, the scaling impacts directly on the precision of the measurements. This illustrates the importance of combining data from different sources to interpret effectively the PS displacement results. At least in what concerns the monitoring of landslide induced surface deformation, without ground-truthing the highly sensitive, millimetric precision PS data, appear prone to misinterpretations.

Although the registered movements are very slow, the observed spatial differences in LOS velocities are significant (Figs. 7 and 8). For example, the PS data indicate that:

– the town of Triesenberg is characterised by higher displacement rates than those in Triesen and this may be in part related to greater slope inclinations. For instance the areas immediately down slope and upslope the centre of Triesenberg, with slopes exceeding 20°, move at LOS velocities −10–11 mm/yr. The site inspection in 2003 revealed that several PS with high velocities coincided with the damaged buildings (Fig. 10);

– the lower part of the landslide complex, in the northern periphery of Triesen, is also characterised by lower PS LOS velocities (typically around −5 mm/yr); this can be in part linked to the low slope inclinations amounting to 6–7°;

– the considerable variation in LOS PS velocity within the Triesenberg urban area appears to be closely related to the varying slope inclinations (Fig. 10). This is well illustrated in Fig. 11 by comparing the changes in PS velocities along a longitudinal (down slope) topographic profile. In particular, in the nearly flat and central portion of the town the PS velocities are the lowest (around 4–5 mm/yr), whereas in the adjacent steep areas (inclinations exceeding 20°), above and below the town centre, the velocities are typically in the range of 8–11 mm/yr. At least 80% of the difference in PS velocities can be accounted for by assuming the presence of slope parallel movements and simply taking into account the local topographic (slope) variations. This in turn strongly suggest that indeed the landslide movements are predominantly translational, as postulated on the basis of ground and subsurface investigations (cf. Fig. 4).

– the central part of the landslide (e.g. at Triesenberg) appears to move at higher velocities with respect to its lateral portions. This may not be related to differences in slope, because the inclinations along the flanks of the landslide are similar to those in the axial part of the mass movement.

In addition to the observed spatial differences in LOS velocities, the deformation time series of some PS revealed the presence of temporal variations in deformation rates. For example Fig. 10 B highlights different

average deformation rates in years 1997, 1998 and 1999 and indicate that the temporal evolution of movements is non-uniform in time. Nevertheless, much caution is needed while interpreting temporal variations in deformation rates, especially when dealing with very slow displacements. Clearly, the precisions on a single measurement and the amount of the observed change have to be taken into account.

Furthermore, a closer examination of Figs. 7 and 8 indicates some additional features of interest that could be exploited in slope stability investigations. In particular, a densely vegetated valley slope area to the south of the main landslide contains some PS, which indicate the presence of deformations. Although neither ground truth nor in situ measurements are available, the examination of the airphotos suggests that these PS could be located on what appear to be an unstable slope deposit. This example illustrates the potential usefulness of the PS technique for recognition of previously unknown, potential landslide hazard areas. In this particular case the presence of a couple of PS only does not allow any finer characterisation (e.g. identification of boundaries of the unstable area).

In summary, this case study illustrates that the PS technique can provide very useful results on an Alpine valley scale, especially where slope hazards originate from large, slowly moving landslides. Thanks to the high density of natural PS targets (~ 120 PS/km^2) it was not only possible to detect and delimit the unstable area, but also to identify some zones within the Triesenberg–Triesen landslide characterised by different displacement rates, and thus by different degree of hazard. The presence of spatially variable displacement rates is not surprising considering the size and composite nature of the landslide, local variations in slope inclinations, decrease in slide thickness away from the central part of the mass movement and presumably better drainage near the slide flanks. The differences in movement rates can also be linked to local lithologic and hydrogeologic variations as well as man's activity e.g. cutting, filling and slope loading related to housing and infrastructure development, increased water input into the more densely urbanised portions of the landslide.

Furthermore, as illustrated in Fig. 11, a careful examination of PS LOS velocity data together with a detailed topographic information can lead to a preliminary distinction between predominantly translational and rotational landslides or slope movements. Where the outcomes can be checked against the available ground data, some additional inferences are possible. In particular, by taking into account the landslide subsurface geometry (Fig. 4) and the slope surface topography (Fig. 11), one can note that the observed variations of PS LOS velocities at Triesenberg agree better with the shape of the main basal shear boundary rather than with the upper secondary slip surfaces.

Finally, the above case study suggests that the PS information can also be very helpful while planning new or upgrading existing in situ monitoring systems. For instance, the PS displacement results can be used to improve the levelling or GPS surveying networks by relocating or adding new measurement points or reference stations (cf. Colesanti et al., 2001). Similarly, through the identification of areas with anomalous or high velocity movements, the PS data can be useful for locating new borehole inclinometers.

6. Discussion and conclusions

The exploitation of SAR data for landslide assessment remains challenging because of the inherent limitations of current space observation systems and relevant data processing techniques. We can identify several requirements for the practical applicability of the conventional DInSAR technique to landslide monitoring, in relation to slope failure size, surface cover, slope inclination, velocity of displacement and mechanism (Wasowski et al., 2002):

1) slide size (minimum dimension) about an order of magnitude larger than the resolution of an imaging sensor;
2) bare surface or with little vegetation;
3) low to moderate slope inclination and suitable orientation with respect to the SAR viewing angle (e.g. for ERS, facing the radar can cause problems of geometrical distortion in SAR images, such as foreshortening and layover effects; these problems can partially be overcome by using satellite acquisitions from both ascending and descending orbits);
4) extremely slow to very slow movements (cf. Cruden and Varnes, 1996);
5) "coherent" landslides, i.e. with little internal deformation (e.g. block slides and in general, deep-seated phenomena);

The innovative PS technique overcomes some of the conventional DInSAR limitations and is capable to provide valuable, high precision ground surface deformation data. Although the technique represents a fully operational tool, its applicability depends on the availability of a sufficient number of suitable targets. Densely urbanised areas (e.g. large towns and cities) with limited vegetation cover represent ideal settings.

In general, the number and the spatial distribution of potential PS is difficult to anticipated a priori, i.e. before acquisition and initial processing of several SAR images. The main reason is that the exact nature and physical principles of scatterers behaviour are still insufficiently known, even though remarkable progresses have been recently reported at least for urban PS (Ferretti et al., 2005; Perissin et al., 2005). It appears, however, that some practical solutions to this problem may soon become available thanks to the growing number of the PS case studies regarding different environmental settings. Nevertheless, for any given area of interest, out of the total PS sample, only some scatterers may be located at or near features of geological significance. This is an important limitation with respect to ground surveying, where the positions of targets to be monitored are carefully selected.

With particular reference to landslide assessment/monitoring, under suitable environmental conditions and with sufficient density of radar targets, the most advantageous aspects of the PS approach are:

a. The cost-effectiveness for wide-area (hundreds and thousands of km^2) applications, typical of space-borne remotely sensed data.
b. The high density of benchmarks (up to several hundreds per km^2).
c. The use of "natural" benchmarks not requiring deployment and maintenance.
d. The possibility of geo-locating the benchmarks with a precision in the order of 1–5 meters.
e. The availability of the extremely valuable ESA ERS archive spanning over 10 years, which enables to carry out retrospective studies. Furthermore, the results of recent studies proved the feasibility of combining new radar data from ENVISAT (satellite launched on March 2002) within ERS PS analyses, despite slight differences in critical image acquisition parameters (Arrigoni et al., 2003; Duro et al., 2003). This ensures the continuation of the ESA ERS archive for the next years.
f. Regular revisiting time in the order of 20–40 days.

On the other hand, the main limitations of the PS approach are linked to:

a. A capability to provide one dimensional deformation data (projection of the 3D displacement) along the sensor-target Line Of Sight. One of the consequences is a direct influence of the slope aspect on the system sensitivity and on the precision of the measurements of translational deformations affecting the slope.
b. A limited range of detectable displacement velocities (usually up to 10–20 cm/yr).
c. A reliance on natural benchmarks implies that their position cannot be chosen freely in advance.
d. In the absence of rock outcrops and/or at least isolated man-made structures, the PS density drops to zero.

The last two limiting factors can be partially circumvented, using passive metallic structures to create "artificial" PS in positions of particular interest. Of course, in this case, the SAR data gathered prior to the installation will not provide valid measurements for the new artificial PS. Moreover, ongoing research as well as future SAR dedicated missions will help to reduce significantly the other limitations of the PS approach. In particular, combining the results of PS analyses carried out with different acquisition geometries will allow, in principle, the reconstruction of full 3D deformation data (Rocca, 2003). Furthermore, involving also lower frequency L-band data allows one to monitor roughly four times faster surface deformations (of course also the precision of the measurements, in terms of standard deviation, will be approximately four times worse). Combined with shorter revisiting times and with modelling data reflecting the spatial correlation of the ground deformations at hand, this will push even further the upper detection limit of the deformation velocity.

A separate issue concerns difficulties in interpreting the exact geotechnical significance of very small, radar sensed ground surface deformations, especially where ground truth is lacking. Although any ground deformation is potentially of interest to an engineering geologist, in the case of landslides, change detection in both vertical and horizontal distances is needed to evaluate landslide mechanisms. However, with their high radar viewing angles, the current space-borne systems can detect only a fraction of a horizontal component of movement.

Nevertheless, the results from the study of the Triesenberg landslide show that when the PS density is high enough, the interferometric products alone (LOS velocities plus DEM) can be used to provide useful information on the predominant movement mechanism, i.e. translational versus rotational. In the former case the PS LOS velocities should correlate well with slope surface inclinations. For rotational movements a general inversion of sign of LOS displacements is expected, corresponding to a change from the downward movements in a slide head area to the upward movements in a slide toe. This has already been observed by Colesanti et al. (2003a) in the case of the large, deep-seated Ancona landslide (Italy).

In general, ground control will always be needed because, in addition to landslide processes, there are several other more or less localised ground deformation phenomena that have to be taken into account to interpret correctly the significance of deformations detected from DInSAR (cf. Wasowski and Gostelow, 1999; Wasowski et al., 2002). These include subsidence (whether caused by natural processes such as compaction, thawing, or man-made), settlement of engineering structures, and shrink and swell of some geological materials.

The additional specific geological aspects that constrain the applicability of SAR data and their interpretation have been discussed by Wasowski and Gostelow (1999). They include:

- The three main phases of landslide movements (pre-failure, during failure and post-failure).
- The importance of gravity and continuous creep.
- The weathering and shallow seasonal creep.

Regarding the pre-failure movements, in the case of brittle geological materials, the displacements can accelerate quickly at the onset of failure and hence will not be suitable for SAR applications. However, in more plastic materials with flat-topped stress-strain curves and with a correspondingly slower onset to failure the movements might be more easily detected by remote sensing techniques.

The movements during a first-time slide occur quickly in comparison to pre- and post-failure deformation phases. The actual rate of displacement will largely depend on the shape of the stress curve of the materials involved. However, in both brittle and plastic materials, the deformation takes place over a comparatively short timescale in a landslides history and hence it seems unlikely that the displacements will be easily detected and monitored by periodic space-borne remote sensing.

Post-failure movements involve many naturally degraded slopes, especially in clays, where pre-existing shear surfaces are often present and can become reactivated. A common feature of these subsequent movements is their low speed, regardless of whether they are brought about by seasonal water pressure changes or by an alteration in loading on a slipped mass (e.g. Skempton and Hutchinson, 1969). These movements may continue over long time periods, perhaps lasting tens of years. This phase in a landslides movement history is thus probably the easiest to detect through periodic remote imagery. The Triesenberg–Triesen landslide case study presented in this work confirms this notion.

It will be also useful to distinguish between the shallow creep deformations caused by seasonal processes on older, degraded slopes and deformations related to deeper seated gravity or continuous creep which take place following unloading or stress relief through down-cutting and erosion in younger geomorphological terrains. Weathering processes may also contribute to shallow deformations on older, more degraded slopes which may already have a surface layer of colluvium.

In conclusion, the PS technique combines the wide-area coverage typical of satellite imagery with the capability of providing displacement data relative to individual image pixels. The larger the area investigated (thousands of km^2), the more cost-effective is the PS monitoring of unstable slopes. At present, however, only very slow ground surface displacements can be measured with mm precision by PS SAR interferometry. Thus it appears that the most attractive and proved contribution provided by this remote sensing technique lies in the possibility of (i.) wide-area qualitative distinction between stable and unstable hillslope areas and (ii.) qualitative hazard zonation of large, very slow landslides based on the identification of segments characterised by different movement rates. Since only the LOS projection of the displacements is detected, a quantitative exploitation of the PS technique is feasible only where adequate in situ data are available. The satellite data will be especially valuable where no other data sources are available by providing initial (potentially wide-area) assessments of ground deformation susceptibility. Then this information can be used to focus on those slopes where there is a potential hazard and where more detailed geotechnical investigations or in situ monitoring may ultimately be required. In slope specific investigations the PS data can represent a very useful complementary data source with respect to the information acquired through ground based observations and in situ surveying. However, the difficulties associated with the feasibility assessments of the applicability of SAR data to local scale problems, as well as with their subsequent interpretation will require a close collaboration between landslide experts and specialists in advanced processing of radar satellite data.

Acknowledgements

We thank Dr. A. Ferretti, Prof. C. Prati and Prof. F. Rocca as well as the whole T.R.E. staff, in particular Eng. A. Fumagalli. Eng. R. Ratti cooperated intensively in carrying out the PS analysis on the Triesenberg–Triesen landslide that was initially performed in the framework of the EC project MUSCL (EVG1-CT-1999-0008). The project was coordinated by Prof. H. Rott (IMGI Universität Innsbruck) with the support of Dr. T.

Nagler. In the framework of the MUSCL activities, sincere thanks are due to GEOTEST A.G., in particular Dr. S. Liener, for the fruitful co-operation. We are also grateful to Paul Kindle of the Tiefbauamt Vaduz (Fürstentum Liechtenstein) for providing the aerial photography and ground surveying information and to Dr. Riccardo Bernasconi and Kaspar Papritz (Sargans, Switzerland) for the in situ monitoring data. We thank Vincenzo Del Gaudio, Stewart Marsh and an anonymous reviewer for their helpful comments. Paul Gostelow, Francesco Palazzo and Vern Singhroy provided useful suggestions on the early version of the manuscript. The efforts of JW were supported in part by the Italian Space Agency (Contract ASI I/R/073/01).

References

Allemann, F., 2002. Erläuterungen zur Geologischen Karte des Fürstentums Liechtenstein 1:25000. Vaduz, Regierung Fürstentum Liechtenstein.

Amelung, F., Galloway, D.L., Bell, J.W., Zebker, H.A., Laczniack, R.J., 1999. Sensing the ups and downs of Las Vegas: InSAR reveals structural control of land subsidence and aquifer-system deformation. Geology 27, 483–486.

Arrigoni, M., Colesanti, C., Ferretti, A., Perissin, D., Prati, C., Rocca, F., 2003. Identification of the location phase screen of ERS-ENVISAT Permanent Scatterers. Proceedings of the third International Workshop on ERS SAR Interferometry (FRINGE 2003), Frascati (Italy), 2–5 December. ESA SP-550 available also online: http://earth.esa.int/fringe03/proceedings/.

Berardino, P., Fornaro, G., Fusco, A., Galluzzo, D., Lanari, R., Sansosti, E., Usai, S., 2001. A new approach for analyzing the temporal evolution of Earth surface deformations based on the combination of DifSAR interferograms. Proceedings of the IEEE International Geoscience and Remote Sensing Symposium (IGARSS 2001), Sydney (Australia), 9–13 July 2001, vol. 6, pp. 2551–2553.

Berardino, P., Fornaro, G., Lanari, R., Sansosti, E., 2002. A new algorithm fro surface deformation monitoring based on small baseline differential SAR interferograms. IEEE Transactions on Geoscience and Remote Sensing 40 (11), 2375–2383.

Berardino, P., Constantini, G., Franceschetti, G., Iodice, L., Pietranera, L., Rizzo, V., 2003. Use of differential SAR interferometry in monitoring and modelling large slope instability at Matera (Basilicata, Italy). Engineering Geology 68/1–2, 31–51.

Bovenga, F., Refice, A., Nutricato, R., Guerriero, L., Chiaradia, M.T., 2004. SPINUA: a flexible processing chain for ERS / ENVISAT long term interferometry. Proceedings of the ESA-ENVISAT Symposium, 6–10 September, 2004, Salzburg, Austria, European Space Agency (ESA) publication SP-572 (CD-Rom).

Bovenga, F., Nutricato, R., Refice, A., Wasowski, J., 2006. Application of multi-temporal differential interferometry to slope instability detection in urban/peri-urban areas. Engineering Geology 88, 219–240.

Carnec, C., Delacourt, C., 2000. Three years of mining subsidence monitored by SAR interferometry, Gardanne, France. Applied Geophysics 43, 43–54.

Carnec, C., Massonnet, D., King, C., 1996. Two examples of the application of SAR interferometry to sites of small extent. Geophysical Research Letters 23, 3579–3582.

CEOS DMSG, 2002. Earth observation for landslide hazard support. The use of Earth Observing Satellites for Hazard Support: Assessments and Scenarios: Final Report of the Committee on Earth Observation Satellites— Disaster Management Support Group. available online: http://disaster.ceos.org/DMSGFinalReport.cfm.

Colesanti, C., Wasowski, J., 2004. Satellite SAR interferometry for wide-area slope hazard detection and site-specific monitoring of slow landslides. Proceedings of the ninth International Symposium on Landslides, Rio de Janeiro (Brazil), 28 June– 2 July 2004, vol. 1, pp. 795–802.

Colesanti, C., Ferretti, A., Prati, C., Rocca, F., 2001. Comparing GPS, optical levelling and Permanent Scatterers. Proceedings of the IEEE International Geoscience and Remote Sensing Symposium (IGARSS 2001), Sydney, 9–13 July, 2001, vol. 6, pp. 2622–2624.

Colesanti, C., Ferretti, A., Prati, C., Rocca, F., 2002. Full exploitation of the ERS archive: multi data set Permanent Scatterers analysis. Proceedings of the IEEE International Geoscience and Remote Sensing Symposium (IGARSS 2002), Toronto (Canada), 24–28 June 2002, vol. 2, pp. 1234–1236.

Colesanti, C., Ferretti, A., Prati, C., Rocca, F., 2003a. Monitoring landslides and tectonic motion with the Permanent Scatterers technique. Engineering Geology 68/1–2, 3–14.

Colesanti, C., Ferretti, A., Novali, F., Prati, C., Rocca, F., 2003b. SAR monitoring of progressive and seasonal ground deformation using the Permanent Scatterers technique. IEEE Transactions on Geoscience and Remote Sensing 41, 1685–1700.

Colesanti, C., Ferretti, A., Locatelli, R., Savio, G., 2003c. Multi-platform Permanent Scatterers analysis: first results. Proceedings of the second IEEE/ISPRS Joint Workshop on Remote Sensing and Data Fusion over Urban Areas, Berlin (Germany), 22–23 May 2003, pp. 52–56.

Costantini, M., Malvarosa, F., Minati, F., Pietranera, L., 2001. Optimal combination of multiple SAR differential interferometric measurements for monitoring terrain displacements. Proceedings of the first IEEE/ISPRS Joint Workshop on Remote Sensing and Data Fusion over Urban Areas, Rome (Italy), 8–9 November 2001, pp. 53–57.

Costantini, M., Malvarosa, F., Minati, F., Pietranera, L., Milillo, G., 2002. A three-dimensional phase unwrapping algorithm for processing of multitemporal SAR interferometric measurements. Proceedings of the IEEE International Geoscience and Remote Sensing Symposium (IGARSS 2002), Toronto (Canada), 24–28 June 2002, vol. 3, pp. 1741–1743.

Crosetto, M., Crippa, B., Monserrat, O., Agudo, M., Biescas, E., 2005. Land subsidence measurement with SAR interferometric data. Proc. of the 2004 Envisat and ERS Symposium, Salzburg, Austria, 6–10 Sept. 2004, ESA SP-572 (CD ROM).

Cruden, D.M., Varnes, D.J., 1996. Landslide types and processes. In: Turner, A.K., Schuster, R.L. (Eds.), Landslides. Investigation and mitigation. Transportation Research Board Spec. Rep., vol. 247. Nat. Academy Press. 673 pp.

Daito, K., Ferretti, A., Kuzuoka, S., Novali, F., Panzeri, P., Rocca, F., 2003. L-band PS analysis: Jers-1 results and TerraSAR-L predictions. Proceedings of the third International Workshop on ERS SAR Interferometry (FRINGE 2003), Frascati (Italy), 2–5 December 2003. ESA SP-550, available also online: http://earth.esa.int/fringe03/proceedings/.

Dehls, J.F., Basilico, M., Colesanti, C., 2002. Ground deformation monitoring in the Ranafjord area of Norway by means of the

Permanent Scatterers technique. Proceedings of the IEEE International Geoscience and Remote Sensing Symposium (IGARSS 2002), Toronto (Canada), 24–28 June 2002, vol. 1, pp. 203–207.

Duro, J., Inglada, J., Closa, J., Adam, N., Arnaud, A., 2003. High Resolution Differential Interferometry Using Time Series of ERS and Envisat SAR Data. Proceedings of the third International Workshop on ERS SAR Interferometry (FRINGE 2003), Frascati (Italy), 2–5 December 2003. ESA SP-550, available also online: http://earth.esa.int/fringe03/proceedings/.

Farina, P., Colombo, D., Fumagalli, A., Manunta, P., Moretti, S., 2004. Landslide Risk Analysis by means of Remote Sensing Techniques: Results from the ESA/SLAM Project. Proceedings of the IEEE International Geoscience and Remote Sensing Symposium (IGARSS 2004), Anchorage (USA), 20–24 September 2004, vol. 1, pp. 62–65.

Ferretti, A., 1997. Generazione di mappe altimetriche da osservazioni SAR multiple, Ph.D. thesis, Politecnico di Milano, Italy.

Ferretti, A., Prati, C., Rocca, F., 1999a. Multibaseline InSAR DEM reconstruction: the wavelet approach. IEEE Transactions on Geoscience and Remote Sensing 37 (2), 705–715.

Ferretti, A., Prati, C., Rocca, F., 1999b. Permanent scatterers in SAR interferometry. Proceedings of the IEEE International Geoscience and Remote Sensing Symposium (IGARSS 1999), Hamburg (Germany), 28 June– 2 July 1999, vol. 3, pp. 1528–1530.

Ferretti, A., Prati, C., Rocca, F., 2000a. Nonlinear subsidence rate estimation using Permanent Scatterers in Differential SAR Interferometry. IEEE Transactions on Geoscience and Remote Sensing 38 (5), 2202–2212.

Ferretti, A., Ferrucci, F., Prati, C., Rocca, F., 2000b. SAR Analysis of Building Collapse by means of the Permanent Scatterers Technique. Proceedings of IEEE International Geoscience and Remote Sensing Symposium (IGARSS 2000), Honolulu (USA), vol. 7, pp. 3219–3221.

Ferretti, A., Prati, C., Rocca, F., 2001a. Permanent Scatterers in SAR Interferometry. IEEE Transactions on Geoscience and Remote Sensing 39 (1), 8–20.

Ferretti, A., Prati, C., Rocca, F., 2001b. Multibaseline phase unwrapping for InSAR topography estimation. Il Nuovo Cimento 124 (1), 159–176.

Ferretti, A., Perissin, D., Prati, C., Rocca, F., 2005. On the physical nature of SAR Permanent Scatterers. Proceedings of the 2005 URSI Commission F Symposium on Microwave Remote Sensing of the Earth, Oceans, Ice, and Atmosphere, Ispra (Italy), 20–21 April 2005, available online: http://ursi-f-2005.jrc.it/proceedings.htm.

Franceschetti, G., Lanari, R., 1999. Synthetic Aperture Radar Processing. CRC Press, New York.

Frommelt, A.G., 1996. Hangbewegungen Triesenberg. Bericht zur GPS Kontrollpunktmessung vom September 1996. Vaduz.

Fruneau, B., Achache, J., Delacourt, C., 1996. Observation and Modeling of the Saint-Etienne-de-Tinée Landslide Using SAR Interferometry. Tectonophysics 265, 181–190.

Gabriel, K., Goldstein, R.M., Zebker, H.A., 1989. Mapping small elevation changes over large areas: differential interferometry. Journal of Geophysical Research 94, 9183–9191.

GEOTEST AG. 1997. Triesenberg, Gefahrenkarte 1:5000, Bericht Prozesse Rutschung und Bodenabsenkung, Bericht Nr. 96172. Zollikofen.

Ghiglia, D.C., Pritt, M.D., 1998. Two-dimensional Phase Unwrapping: Theory, Algorithms and Software. John Wiley & Sons, Inc., New York.

Giordani, L., Panzeri, P., 2003. Elaborazioni di immagini JERS per applicazioni interferometriche. Master degree thesis in Telecommunications Engineering, Politecnico di Milano, Italy.

Hanssen, R.F., 2001. Radar Interferometry: Data Interpretation and Error Analysis. Kluwer Academic Publishers, Dordrecht. 326 pp.

Henderson, F.M., Lewis, A.J. (Eds.), 1998. Principles and Applications of Imaging Radar, 3rd edition. Vol. 2 of Manual of Remote Sensing. John Wiley & Sons, Inc., New York.

Hilley, G.E., Burgmann, R., Ferretti, A., Novali, F., Rocca, F., 2004. Dynamics of slow-moving landslides from Permanent Scatterer analysis. Science 304, 1952–1955.

Hooper, A., Zebker, H., Segall, Kampes, B., 2004. A new method for measuring deformation on Volcanoes and other natural terrains using InSAR persistent scatterers. Geophysical Research Letters 31, L23611.

IGOS GEOHAZARDS, 2004. GEOHAZARDS theme report: For the Monitoring of our Environment from Space and from Earth. European Space Agency (ESA) publication. 55 pp.

Kampes, B.M., Adam, N., 2003. Velocity field retrieval from long term coherent points in radar interferometric stacks. Proceedings of the IEEE International Geoscience and Remote Sensing Symposium (IGARSS 2003), Toulouse (France), 21–25 July 2003, vol. 2, pp. 941–943.

Ketelaar, V.B.H., Hanssen, R.F., 2003. Separation of different deformation regimes using PS-InSAR data. Proceedings of the third International Workshop on ERS SAR Interferometry (FRINGE 2003), Frascati (Italy), 2–5 December 2003. ESA SP-550, available also online: http://earth.esa.int/fringe03/proceedings/.

Kimura, H., Yamaguchi, Y., 2000. Detection of landslide areas using satellite radar interferometry. Photogrammetric Engineering and Remote Sensing 66, 337–344.

Lanari, R., Mora, O., Manunta, M., Mallorqui, J.J., Berardino, P., Sansosti, E., 2004. A small baseline approach for investigating deformations on full resolution Differential SAR Interferograms. IEEE Transactions on Geoscience and Remote Sensing 42, 1377–1386.

Le Mouélic, S., Raucoules, D., Carnec, C., King, C., 2003. A least square adjustments of multitemporal InSAR data: application to the ground deformation of Paris. Photogrammetric Engineering and Remote Sensing 71 (2), 197–205.

Massonnet, D., Feigl, K.L., 1998. Radar Interferometry and its application to changes in the Earth's surface. Review of Geophysics 36, 441–500.

Massonnet, D., Rossi, M., Carmona, C., Adragna, F., Peltzer, G., Feigl, K., Rabaute, T., 1993. The displacement field of the Landers earthquake mapped by Radar Interferometry. Nature 364, 138–142.

Massonnet, D., Briole, P., Arnaud, A., 1995. Deflation of Mount Etna monitored by Spaceborne Radar Interferometry. Nature 375, 567–570.

Massonnet, D., Vadon, H., Rossi, M., 1996. Reduction of the need for phase unwrapping in Radar Interferometry. IEEE Transactions on Geoscience and Remote Sensing 34, 489–497.

Monti Guarnieri, A., 2002. Unpublished university lecture notes on Radar Theory and Technique, Politecnico di Milano, Italy.

Nagler, T., 2002. Monitoring Urban Subsidence, Cavities and Landslides by Remote Sensing (MUSCL). Technical Report WP330 "DInSAR Methods for Alpine Valleys", available online: http://dude.uibk.ac.at/projects/muscl/.

Nagler, T., Rott, H., Kamelger, A., 2002. Analysis of landslides in Alpine Areas by means of SAR Interferometry. Proceedings of the IEEE International Geoscience and Remote Sensing Symposium (IGARSS 2002), Toronto (Canada), 24–28 June 2002, vol. 1, pp. 198–200.

Novali, F., Ferretti, A., Prati, C., Rocca, F., Savio, G., Musazzi, S., 2005. PSInSAR Validation by Means of a Blind Experiment Using Dihedral Reflectors. Proceedings of FRINGE 2005, Frascati (Italy),

28 November– 2 December 2005. ESA SP-610, available also online: http://earth.esa.int/workshops/fringe2005/proceedings/.

Perissin, D., Prati, C., Ferretti, A., 2005. Spaceborne SAR anatomy of a city. Proceedings of FRINGE 2005, Frascati (Italy), 28 November– 2 December 2005. ESA SP-610, available also online: http://earth.esa.int/workshops/fringe2005/proceedings/.

Refice, A., Bovenga, F., Guerriero, L., Wasowski, J., 2001. DInSAR applications to landslide studies. Proceedings of the IEEE International Geoscience and Remote Sensing Symposium (IGARSS 2001), Sydney (Australia), 9–13 July 2001, vol. 1, pp. 144–146.

Rocca, F., 2003. 3D Motion recovery with multi-angle and/or left right Interferometry. Proceedings of the third International Workshop on ERS SAR Interferometry (FRINGE 2003), Frascati (Italy), 2–5 December 2003. ESA SP-550, available also online: http://earth.esa.int/fringe03/proceedings/.

Rosen, P.A., Hensley, S., Joughin, I.R., Li, F.K., Madsen, S.N., Rodriguez, E., Goldstein, R.M., 2000. Synthetic Aperture Radar Interferometry. Proceedings of the IEEE, vol. 88, pp. 333–376.

Rott, H., Scheuchl, B., Siegel, A., Grasemann, B., 1999. Monitoring very slow slope movements by means of SAR interferometry: a case study from a mass waste above a reservoir in the Ötztal Alps, Austria. Geophysical Research Letters 26, 1629–1632.

Rott, H., Mayer, C., Siegel, A., 2000. On the operational potential of SAR interferometry for monitoring mass movements in Alpine areas. Proceedings of the 3rd European Conference on Synthetic Aperture Radar (EUSAR 2000), Munich, Germany.

Sandwell, T., Price, E.J., 1998. Phase gradient approach to stacking interferograms. Journal of Geophysical Research 103 (B12), 30183–30204.

Sharroo, R., Visser, P., 1998. Precise orbit determination and gravity field improvement for the ERS Satellites. Journal of Geophysical Research 103 (C4), 8113–8127.

Singhroy, V., Molch, K., 2004. Characterizing and monitoring rockslides from SAR techniques. Advances in Space Research 33, 290–295.

Singhroy, V., Mattar, K.E., Gray, A.L., 1998. Landslide characteristics in Canada using interferometric SAR and combined SAR and TM images. Advances in Space Research 3, 465–476.

Skempton, A.W., Hutchinson, J.N., 1969. Stability of natural slopes and embankment foundations. State of the Art Report. 7th Int. Conf. Soil Mech. and Found. Eng. , pp. 291–340.

Strozzi, T., Farina, P., Corsini, A., Ambrosi, C., Thüring, M., Zilger, J., Wiesmann, A., Wegmüller, U., Werner, C., 2005. Survey and monitoring of landslide displacements by means of L-band satellite SAR interferometry. Landslides 2 (3), 193–201.

Usai, S., 2002. A least-squares approach for long-term monitoring of deformations with differential SAR interferometry. Proceedings of the IEEE International Geoscience and Remote Sensing Symposium (IGARSS 2002), Toronto (Canada), 24–28 June 2002, vol. 2, pp. 1247–1250.

Usai, S., 2003. A least squares database approach for SAR interferometric data. IEEE Transactions on Geoscience and Remote Sensing 41 (4), 753–760 (part 1).

Van der Kooij, M., 1999. Engineering geology landslide investigations and SAR Interferometry. Proceedings of FRINGE'99, Liege, Belgium. http://www.esa.int/fringe99.

Van der Kooij, M., 2003. Coherent target analysis. Proceedings of the third International Workshop on ERS SAR Interferometry (FRINGE 2003), Frascati (Italy), 2–5 December 2003. ESA SP-550, available also online: http://earth.esa.int/fringe03/proceedings/.

Wasowski, J., Gostelow, P., 1999. Engineering geology landslide investigations and SAR Interferometry. Proceedings of FRINGE'99, Liege, Belgium. http://www.esa.int/fringe99.

Wasowski, J., Singhroy, V. (Eds.), 2003. Remote Sensing and Monitoring of Landslides— Special Issue. Eng. Geol., 68(1–2).

Wasowski, J., Refice, A., Bovenga, F., Nutricato, R., Gostelow, P., 2002. On the applicability of SAR Interferometry techniques to the detection of slope deformations. Proceedings of the 9th IAEG Congress, Durban. published on CD-ROM.

Werner, C., Wegmuller, U., Strozzi, T., Wiesmann, A., 2003a. Interferometric Point Target Analysis for Deformation Mapping. Proceedings of the IEEE International Geoscience and Remote Sensing Symposium (IGARSS 2003), Toulouse (France), 21–25 July 2003, vol. 7, pp. 4362–4364.

Werner, C., Wegmuller, U., Wiesmann, A., Strozzi, T., 2003b. Interferometric Point Target Analysis with JERS-1 L-band SAR Data. Proceedings of the IEEE International Geoscience and Remote Sensing Symposium (IGARSS 2003), Toulouse (France), 21–25 July 2003, vol. 7, pp. 4359–4361.

Zebker, H.A., Goldstein, R.M., 1986. Topographic mapping from Interferometric Synthetic Aperture Radar observations. Journal of Geophysical Research 91 (B5), 4993–4999.

Zebker, H.A., Villasenor, J., 1992. Decorrelation in Interferometric Radar Echoes. IEEE Transactions on Geoscience and Remote Sensing 30, 950–959.

Zebker, H.A., Werner, C.L., Rosen, P.A., Hensley, S., 1994a. Accuracy of topographic maps derived from ERS-1 Interferometric Radar. IEEE Transactions on Geoscience and Remote Sensing 32 (4), 823–836.

Zebker, H.A., Rosen, P.A., Goldstein, R.M., Gabriel, A., Werner, C.L., 1994b. On the derivation of coseismic displacement fields using Differential Radar Interferometry: the Landers earthquake. Journal of Geophysical Research 99 (B10), 19617–19634.

Zebker, H.A., Rosen, P.A., Hensley, S., 1997. Atmospheric effects in Interferometric Synthetic Aperture Radar Surface Deformation and topographic maps. Journal of Geophysical Research 102 (B4), 7547–7563.